POLITECNICO DI TORINO

Collegio di Ingegneria Chimica e dei Materiali

Master of Science Course in Materials Engineering for Industry 4.0

Master of Science Thesis

Analysing the influence of the workpiece geometry on the coolant flow field distribution during the milling process with internal coolant supply



Tutors

Prof. Daniele Ugues

Prof. Milena Salvo

Candidate

Md Ibthisum Alam

Settembre 2025

Erasmus Mundus Joint Master in Manufacturing 4.0 by intElligent and susTAinable technologies



MASTER's Degree Thesis

Analysing the influence of the workpiece geometry on the coolant flow field distribution during the milling process with internal coolant supply

Supervisors

Prof. Dr.-Ing. Martin DIX

Dr.-Ing. Matthias REHM

Prof. Cédric COURBON

Prof. Daniele UGUES

Candidate

Md Ibthisum ALAM

September 2025













Abstract

In the context of sustainable manufacturing, an efficient coolant delivery system is essential to minimize tool wear while maintaining the machined surface quality. The cooling performance, however, strongly varies depending on operating parameters and tool-workpiece interaction. The current study addressed this issue and developed a Computational Fluid Dynamics (CFD) model to evaluate coolant flow behavior in internally cooled milling. The simulations from the model were tested against surrogated experimental rigs, and the comparison showed good agreement. The analysis was based on the Design of Experiments (DOE) framework, particularly Central Composite Design (CCD), where the influence of three factors, namely workpiece geometry (flat vs. curved), rotational speed (250-750 RPM) and coolant flow rate (20-30 l/min), on four performance metrics such as average coolant velocity, coolant volume fraction, coolant coverage area, and turbulence kinetic energy (TKE) were investigated. A preliminary assessment on the influence of coolant type was also executed, and water and water-based semi-synthetic coolant showed almost identical results, deviating within the range of 1-2%. The DOE outputs demonstrated the dominance of coolant flow rate on enhancing jet momentum and turbulence intensity, while workpiece geometry heavily defined the coolant retention and distribution, with curved geometries consistently obtaining superior results. Rotational speed had a lesser yet significant impact as higher spindle speed (750 RPM) improving velocity and turbulence, but at the same time, diminishing coolant volume fraction and coverage. Regarding interaction effects, any involvement of geometry was found to be significant, highlighting the need for geometry-specific optimization strategies. Through the study, a validated CFD-DOE framework was established for analyzing coolant delivery in milling. The insights obtained are directly transferable to tool design and process planning, hence providing scope for geometry-adaptive cooling strategies for advanced manufacturing.

Keywords: End Milling, Computational Fluid Dynamics (CFD), Multiphase Flow, Design of Experiments (DOE).

Acknowledgments

The thesis has truly been a fruitful and satisfying experience and I would like to sincerely acknowledge all the people who have helped me in every possible way to make this happen.

Starting from my respected supervisors at Technische Universität Chemnitz, Prof. Dr.-Ing. Martin Dix and Dr.-Ing. Matthias Rehm, I deeply thank them for organizing and structuring the thesis and providing me with the opportunity to conduct research in this area. I am profoundly grateful to my mentor Mr. Steffen Brier, for providing me with the clear and detailed guideline to proceed with the thesis. Having such a skilled person in the field of Computational Fluid Dynamics (CFD) by my side was a blessing and from our weekly meeting every week, I learnt a lot from him. I would also like to mention my great appreciation for Dr.-Ing. Joachim Regel, who was always available to help me with valuable advice. I cannot thank everyone from the Professorship Production Systems and Processes enough, including Ms. Katja Klöden; their support and kindness made my time at the professorship a very enjoyable and memorable one. Special thanks to Prof. Dr.-Ing. Stephan Odenwald, for making a smooth thesis experience at Technische Universität Chemnitz. His session on conducting the research and writing the thesis helped me a lot and kept me in the right direction.

Additionally, I would like to extend my heartfelt gratitude to my supervisors at other institutions including Prof. Cédric Courbon from Ecole Nationale d'Ingénieurs de Saint-Étienne (ENISE), and Prof. Milena Salvo and Prof. Daniele Ugues from Politecnico di Torino, for their regular assistance and for providing the resources necessary to conduct this research. I would also like to thank Dr. Aurélie Brayet for her constant help, not only with the organizational aspect of the thesis but throughout my entire master's duration. My parents, Ms. Rokeya Begum and Mr. Md Jahangir Alam, have been a part of this journey as much as I am, and I cannot express in words to explain how grateful I am for the support and sacrifices they have made.

Table of Contents

Chapter 1	Introduction and Background	1
1.1. Intro	duction	1
1.2. Resea	arch Motivation and Aims	2
1.3. Resea	arch Questions	4
1.4. Organ	nization of the Thesis	5
Chapter 2	Literature Review	6
2.1. Overv	view of End Milling and Coolant Supply	6
2.2. Comp	outational Fluid Dynamics in Machining	10
2.3. Inter	nal Cooling Channel Design and Optimization	15
2.4. Resea	arch Gap and Summary	18
Chapter 3	Methodology	20
3.1. Resea	arch Design	20
3.2. CFD N	Model Development	22
3.3. Desig	n of Experiments (DOE) Framework	29
3.4. Mode	l Validation Approach	32
Chapter 4	Results and Discussion	35
4.1. Mode	l Validation with Experiments	35
4.2. Mesh	Independence Test	37
4.3. Influe	ence of Coolant Type	40
4.4. Influe	ence of Operating Parameters and Geometry (DOE Analysis)	42
4.4.1.	Analysis of Average Coolant Velocity	42
4.4.2.	Analysis of Coolant Volume Fraction	45
4.4.3.	Analysis of Coolant Coverage Area (%)	48
4.4.4.	Analysis of Turbulence Kinetic Energy (TKE)	51

4.4.5. Summary of DOE Results	54
Chapter 5 Conclusion and Future Work	56
Appendix A	59
Appendix B	61
Bibliography	63

List of Figures

Figure 2.1: Supply of cutting fluids in external and internal cooling methods [20].	8
Figure 2.2 : Coolant volume fraction in the drilling simulation developed by Johns	et al.
[7].	11
Figure 2.3: Comparison of experimental and simulated coolant flow in the stud	y by
Bräunig et al. [33].	11
Figure 2.4: Volume fraction of coolant Flow noted in the study by Brier et al.[36].	12
Figure 2.5 : Comparison of fluid volume distribution from the study of Biermann	and
Oezkaya [40].	13
Figure 2.6: Comparison of fluid velocity distribution from the study of Zachert et al.	[41].
	14
Figure 2.7 : Streamline of cutting fluid, outlet pressure and velocity distributio	n as
reported by Peng et al.[42].	14
Figure 2.8: Velocity profiles from CFD analysis of internal cooling channels with var	ying
transition radii, based on the findings of Kelliger et al. [45].	16
Figure 2.9 : Cutting fluid supply at different nozzle orientations [20].	17
Figure 3.1: Methodology flowchart for CFD analysis and coolant optimization.	21
Figure 3.2 : (a) Original Harvi Ultra 8X tool [52] and (b) simplified tool geometry	with
coolant channels.	23
Figure 3.3 : CFD model setup in ANSYS showing the fluid domain (200 \times 200 \times 200 in	mm)
containing the milling tool, workpiece, and mounting plate.	24
Figure 3.4: (a) Global mesh view and (b) Localized refinement near coolant inlets.	24
Figure 3.5 : Domain setup for CFD simulation.	26
Figure 3.6: Reference plane positioned at the cutting zone for coolant flow evalua	ation
(a) Flat Workpiece (b) Curved Workpiece.	28
Figure 3.7: Power consumption versus coolant flow rate for various milling to	ools,
highlighting the HARVI™ Ultra 8X [56].	30
Figure 3.8 : Experimental Setup: (a) DECKEL MAHO DMC 850 V CNC Vertical Machi	ning
Center and (b) The coolant pump system.	32
Figure 3.9 : Tools Used in experiment.	33
Figure 4.1: Experimental vs. CFD comparison for Tool 1	36

Figure 4.2: Experimental vs. CFD comparison for Tool 2.	36
Figure 4.3: Experimental vs. CFD comparison for Tool 3.	37
Figure 4.4 : Percentage deviation of coarse and fine mesh results relative to the med	lium
mesh for key flow parameters.	39
Figure 4.5 : Comparison of water and semi-synthetic coolant for (a) Average velocity	ocity
(m/s), (b) Volume fraction, (c) Coverage area (%), and (d) Turbulence kinetic en	ergy
(m^2/s^2) .	41
Figure 4.6: Comparison of coolant streamlines for (a) water and (b) semi-synt	hetic
coolant under identical conditions, indicating negligible impact of coolant type on	flow
behavior.	41
Figure 4.7: Comparison of coolant volume fraction renderings for (a) water and (b) s	emi-
$synthetic\ coolant\ under\ identical\ conditions, indicating\ negligible\ impact\ of\ coolant$	type
on flow behavior.	42
Figure 4.8: Pareto chart of standardized effects for average coolant velocity.	43
Figure 4.9: Main effect plots for average coolant velocity.	44
Figure $4.10:$ (a) Surface plot of average coolant velocity (m/s) for flat workpiece	. (b)
Contour plot of average coolant velocity (m/s) for flat workpiece.	45
Figure $4.11:$ (a) Surface plot of average coolant velocity (m/s) for curved workpiece	e. (b)
Contour plot of average coolant velocity (m/s) for curved workpiece.	45
Figure 4.12 : Pareto chart of standardized effects for average coolant volume frac	tion.
	46
Figure 4.13: Main effect plot for average coolant volume fraction.	47
Figure 4.14 : (a) Surface plot of average coolant volume fraction for flat workpiece	. (b)
Contour plot of average coolant volume fraction for flat workpiece.	47
Figure 4.15 : (a) Surface plot of average coolant volume fraction for curved workp	iece.
(b) Contour plot of average coolant volume fraction for curved workpiece.	48
Figure 4.16: Pareto chart of standardized effects for coolant coverage area (%).	49
Figure 4.17: Main effect plots for coolant coverage area (%).	50
Figure 4.18 : (a) Surface plot of coolant coverage area (%) for flat workpiece. (b) Con	tour
plot of coolant coverage area (%) for flat workpiece.	50
Figure 4.19: (a) Surface plot of coolant coverage area (%) for curved workpiece	. (b)
Contour plot of coolant coverage area (%) for curved workpiece.	51

Figure 4.20 : Pareto chart of standardized effects for turbulence kinetic energy	(TKE).
	52
Figure 4.21: Main effect plots for turbulence kinetic energy (TKE).	53
Figure 4.22 : (a) Surface plot of turbulence kinetic energy (m^2/s^2) for flat workpi	ece. (b)
Contour plot of turbulence kinetic energy (m^2/s^2) for flat workpiece.	53
Figure 4.23 : (a) Surface plot of turbulence kinetic Energy (m^2/s^2) for curved workpiece.	
(b) Contour plot of turbulence kinetic energy (m^2/s^2) for curved workpiece.	54

List of Tables

Table 3.1: Geometrical specifications of the modeled end mill tool.	22
Table 3.2 : CFD meshing parameters and settings.	25
Table 3.3 : Summary of boundary conditions used in the CFD simulation.	27
Table 3.4 : Solver control settings.	27
Table 3.5: Physical properties of water and water-based semi-synthetic coolant	[55].29
Table 3.6 : DOE factors and levels.	30
Table 3.7 : DOE simulation matrix showing the factor levels for workpie	ce type,
rotational speed, and coolant flow rate.	32
Table 3.8: Calculated flow rates (l/min) for each tool based on measured coolant	volume
and time.	34
Table 4.1: Element sizes and mesh counts for each mesh level.	38
Table 4.2 : Key coolant flow metrics for each mesh level.	39
Table 4.3: ANOVA P-value summary for average coolant velocity.	43
Table 4.4 : ANOVA P-value summary for average coolant volume fraction.	46
Table 4.5: ANOVA P-value summary for coolant coverage area (%).	49
Table 4.6: ANOVA P-value summary for turbulence kinetic energy (TKE).	52
Table 4.7 : Summary of factor significance across response metrics (+ = positive	effect, -
= negative effect).	55

Nomenclature

Abbreviations & acronyms

ANOVA Analysis of Variance

CCD Central Composite Design

CFD Computational Fluid Dynamics

CFRP Carbon fiber Reinforced Plastic

DOE Design of Experiments

FSI Fluid-Structure Interaction

HPC High-pressure Cooling

MRR Material Removal Rate

RSM Response Surface Methodology

RPM Revolutions Per Minute

RMS Root Mean Square

SLM Selective Laser Melting

SST Shear Stress Transport

TKE Turbulence Kinetic Energy

Symbols

- A Coolant coverage area (%)
- a Flow speed (m/s)
- Δt Time step (s)
- Δx Cell size (m)
- ε Turbulent dissipation rate

- f Volume force
- k Turbulence kinetic energy (m^2/s^2)
- η Dynamic viscosity
- p Pressure (Pa)
- Q Volumetric flow rate (l/min)
- ρ Fluid density (kg/m³)
- φ Coolant volume fraction
- t Time (s)
- υ Velocity (m/s)
- V Average coolant velocity (m/s)
- ω Specific dissipation rate
- x, y, z Spatial directions
 - m Mass flow rate (kg/s)

Constants

g Acceleration due to gravity (9.81 m/s^2)

Chapter 1

Introduction and Background

1.1. Introduction

In the modern manufacturing context, machining plays a pioneering role by generating the parts production with precise dimensions, shapes and surface finishes through the material removal in the form of chips. Among the processes, milling is considered one of the most versatile and widely used machining techniques because of its enhanced flexibility achieved through the multi-axis cutting capabilities [1]. However, high-speed milling characterized by intense plastic deformation and friction at the tool-workpiece contact zone results in the conversion of nearly all input energy up to 99% into heat energy [2].

While machining high-strength or heat-resistant alloys, the issue becomes serious as it introduces the complexities of increased tool wear, thermal distortion of the workpiece, and dimensional inaccuracies. Cutting fluids or commonly known as coolants, are utilized to address these challenges and they resolve the issue by moving away the heat from the cutting zone, reducing the friction, facilitating chip evacuation, and extending the tool life.

It is well proven that coolants can have a significant role in improved machining and increased material removal rates (MRR), particularly when pumped through advanced methods like internal coolant supply systems. Compared to the widely adopted external systems, coolants flow from the optimized internal channel structure directly to the cutting edge [3]. This ensures higher cooling efficiency, reduced thermal loads, and better lubrication at critical interfaces [4]. The overall effectiveness of the system, however, is determined by several factors such as the tool rotation, coolant flow rate, and the workpiece shape, each of which can influence the fluid flow patterns and thermal behavior. As the demand for high-performance machining of advanced materials in industries like aerospace, automotive, and energy is on the rise, the importance of an optimized system of internal coolant supply is gaining momentum.

Internal coolant supply systems are constructed in such a way that cutting fluid reaches directly to the cutting zone through the tool's internal channels. A typical components of

the system include a hydraulic pump, throttle valve, relief valve, flow meter, and filtration unit. To operate effectively, it is important that the system offers adjustable fluid flow, consists of overload protection to control pressure, and supports coolant recovery. It enables the system to cool efficiently, lubricate stably, and make sure the conservation of sustainable aspects during high-performance milling.

A major challenge in the internal cooling supply system is the variation of coolant flow behavior arising from the changes in working geometry and tool operating parameters. Internal channels are designed with the aim of precise coolant flow to the cutting zone, while any alteration in workpiece shape or profile can disrupt the expected flow trajectory, leading to uneven cooling and concentrated heat buildup. In the same way, when the tool rotation or coolant flow rate fluctuates it creates an uncertainty on the coolant's velocity, turbulence, and impact angle. These dynamic interactions create complexity in achieving the optimal cooling and lubrication under diverse machining scenarios. Addressing these challenges is the core research problem explored in this study.

1.2. Research Motivation and Aims

It is well documented that the coolants bring benefits in machining. They provide advantages by significantly prolonging tool life, generating better surface finishes, and enhancing overall performance. But as the tool-workpiece combinations vary and cutting conditions change these advantages are not consistently realized. Additionally, if the coolant is not properly controlled the excessive supply can cause environmental and health concerns, particularly involving the safe disposal and operator safety. These issues contribute largely to the operating costs may sometimes outweigh the potential benefits. As in the modern industry, more emphasis is placed on the sustainability and tightening of environmental regulations, it has become essential that coolant applications be optimized both functionally and economically.

Despite their advantages, the implementation of internal coolant supply systems is still considered a challenge due to a limited understanding of coolant flow interactions with the workpiece under varying operating conditions. This gap often requires expensive and time-consuming experimental trials to evaluate cooling performance across various configurations. In this context, Computational Fluid Dynamics (CFD) can serve as a powerful alternative. This tool not only saves on the costs from the experimental settings

but also improves the quality of analysis by offering detailed visualization and analysis of coolant behavior that is difficult to achieve from an experimental rig. Particularly, to evaluate the morphology of fine-distributed coolant droplets, CFD has shown incredible success, which otherwise can be very challenging or even impossible with experimental measurements. The CFD simulation technique becomes more relevant for intermittent processes like milling, where multiple interactions occur at a time. It was noted from previous studies that the CFD has the potential to act as a highly effective tool when optimizing tool design and improving thermal management in machining [5], [6], [7].

By addressing the gaps in the current manufacturing context and leveraging CFD for predictive modeling, this study aimed to support the development of more efficient and sustainable internal cooling strategies. The outcomes of this research are directly applicable to modern industries and align with the overarching principles of industry 4.0, where simulation-driven design, digital process optimization, and smart cooling integration are central to obtaining high-performance and eco-friendly production.

The primary aim of this thesis was to investigate workpiece geometry and operational conditions' influence on the coolant flow pattern in internally cooled milling operations. The target was to have a better understanding of coolant flow characteristics, optimize the cooling performance, and contribute to the progression of more effective cooling impacts by means of CFD modeling and experimental validation. The specific objectives were as follows:

1. Develop a CFD model to simulate coolant flow in internal cooling setups

This includes the construction of a detailed CFD model replicating the internal coolant flow behavior in milling. The model should also include varying workpiece geometries to observe their effects on coolant volume fraction, coolant velocity, flow field morphology, and turbulence. The developed system should be flexible enough to vary the operating conditions including the tool rotation and coolant flow rate.

2. Validate the CFD results through experimental and literature benchmarks

The simulation accuracy needs to be tested against similar experimental rigs. Under the identical operating parameters, the flow pattern of the coolants has to be compared. The outputs from the simulation should be backed up by the experimental observations.

3. Apply Design of Experiments (DOE) to study and optimize tool and coolant parameters It is important that the crucial input parameters of the study have been identified. Using structured DOE methods, the input variables will be altered to measure their impact on

the cooling performance metrics. The results should be implemented to determine the optimal parameters for effective cooling and would serve as a base for recommendations for future internal cooling systems.

1.3. Research Questions

The study was driven by the need to observe and understand the coolant flow behavior from an internal coolant supply system in milling, which was going through dynamic operations where key machining variables were changing. The following questions, particularly, guided the scope of this research:

1. How does workpiece geometry affect the coolant flow field?

The question explored what role workpiece surface curvature plays in relation to the flow trajectory, velocity and dispersion of coolant within the system. By comparing flow impact on flat and curved geometries the study looked to point out the zones prone to insufficient cooling and develop geometry adaptive cooling strategies.

2. How do variations in rotational speed and coolant flow rate influence turbulence and coolant velocity?

The intensity of the tool rotation and coolant flow rate are critical in evaluating the flow turbulence and direction. This phenomenon introduced the question of which depth these parameters affect the coolant dynamics near the tool-workpiece interface. Investigating this question would be helpful in obtaining insight on controlling flow-induced turbulence to achieve better heat dissipation and chip evacuation.

3. To what extent do CFD simulation results align with experimentally obtained flow field data?

It was important that the developed CFD model could be relied upon to accurately represent the real-world coolant flow behavior. This question addressed this condition and assessed the extent to which the simulation can be trusted. While a direct comparison between the developed CFD model of the mill and experimental tests might not be feasible due to the tool-specific differences, the modeling approach could still be evaluated through surrogate experiments. The goal was to make sure that the constructed model could be utilized to serve as a robust predictive tool for future coolant performance studies.

1.4. Organization of the Thesis

The thesis report is arranged in total five chapters where each chapter was structured in a systematic way to address the research objectives and to generate a comprehensive understanding of internal coolant flow behavior in milling operations.

Chapter 1 starts by introducing the research, outlining the background, motivations, aim and significance of the study. The research questions explored in the study are defined here with an overview of the thesis structure.

Chapter 2 includes a detailed literature review on the existent works on end milling and coolant applications. It also discusses case studies involving the CFD simulations in machining to reshape the research gap explored in this study.

Chapter 3 outlines the methodology followed in this work. The development of the CFD model including tool and workpiece geometry selection, meshing, boundary conditions and solver setup are described in detail. The chapter also explains the Design of Experiments (DOE) adopted, experimental setup and model verification approach.

Chapter 4 demonstrates the results and analysis. It evaluates the research questions in correspondence to the computational model and interprets the findings from the perspective of machining performance and coolant system design.

Chapter 5 concludes the report by pointing out the key results and providing answers to the research questions stated. Highlighting the study's contribution, the chapter acknowledges any possible limitations and provides directions for future research in this field.

Chapter 2

Literature Review

2.1. Overview of End Milling and Coolant Supply

Milling is considered one of the most widely adopted machining technologies due to their great versatility. End milling, in particular, has been present in the vast majority of industries because of its ability to produce high-precision components in the forms of pockets, slots, and contoured surfaces. Unlike drilling, end mill tools come with sharp cutting edges along their length that facilitate the cutting of workpiece from the top, bottom, side, or various angles. This multi-directional machining ability provides milling with a great deal of freedom compared to the other machining techniques [1].

Milling plays a prominent role in shaping the hard-to-cut advanced materials, such as Inconel 718, for aerospace and marine applications. This nickel-based superalloy is well known for its strength, thermal stability, and corrosion resistance at extreme temperatures; however, it is its high strength, low thermal conductivity, and strain hardening behavior that makes machining very difficult [8], [9]. While milling Inconel 718, a substantial heat is generated as elevated temperature affects it very little to soften [10]. This excess heat can initiate thermal damage and alter the machined surface, which in consequence impacts the part's fatigue life. To tackle this issue, high-speed milling has emerged as a promising approach as it offers high machining efficiency, superior surface finish, and cost-effectiveness while maintaining the cutting temperature under a limit [11]. Although high-speed milling has shown desired outcomes for machining hard-to-cut materials such as titanium or Inconel alloys, it is still important that effective cooling is in place to maintain the process stability and tool life [12].

Cutting fluids or coolants play a pivotal role here by controlling the temperature rise as well as improving machining efficiency. In the absence of proper cooling, a considerable portion of the input energy produced as heat can result in the adverse effects of thermal damage, dimensional distortion, micro-cracking, and rapid tool wear [2], [13]. The coolants work as a mitigator by serving three primary purposes: cooling, lubrication, and chip evacuation [3], [14], [15]. Coolants, in their most basic function, absorb and dissipate the heat from the machining interface and help maintain a stable temperature and prolong the tool life. As lubricants, they lower the friction between the cutting edge

and chip by forming a thin layer, generating a smooth and improved machined surface. In addition, coolants flush away chips from the cutting region and prevent tool clogging and built-up edge formation, particularly for the hard-to-cut materials like titanium or Inconel alloys.

The effectiveness of coolants is influenced by their chemical composition, mode of application, and machining conditions. Water for instance, has great cooling capabilities but lacks lubrication that may lead to corrosion in ferrous tools. Better performance was observed by the water-miscible coolants with soluble oil that significantly improves the lubrication [14]. Mineral-oil-based coolants are best employed where lubrication is a concern, but there is a risk of smoke and mist formation at high temperatures, which potentially could impact the safety of the operator [16]. Hence, when selecting the right type of coolant, there has to be a balance between the thermal and lubrication priorities specified for the particular machining parameters. Furthermore, it is important to consider the environmental and economic perspectives of the coolants, given the drawbacks arise from the conventional flood cooling systems. Advanced techniques emphasize optimizing coolant usage while at the same time protecting the machining performance, surface quality, and tool longevity.

The mode of how coolant is delivered has a big impact on evaluating the coolant effectiveness. Traditionally, external flood cooling remains the most dominant approach where coolants, typically water or oil-based, are flooded over the machining zone. This method, however, does not work well during the high-performance machining of difficult-to-cut materials such as titanium or Inconel alloys. The issues observed include low coolant pressure, misaligned nozzle, poor injection angles, and tool rotation, all of which result in insufficient coolant flow to the tool-chip interface. The effect is prominent in parts with intricate geometry, such as deep cavities and integrated impellers. For milling, the machining that involves intermittent cutting, the challenge is even greater as cooling gets disrupted after each cut [17]. Moreover, with flood cooling, high consumption is often involved due to low utilization efficiency. This leads to not only an increase in operating costs but also adds concerns related to their safe disposal [4]. Weinert et al. [18] highlighted the need for efficient cooling techniques, noting that coolant-related expenses may lead up to 7–17% of the total manufacturing cost.

Internal cooling systems can counter these limitations as they have emerged as an efficient and targeted alternative. As shown in Figure 2.1, these systems are embedded with integrated micro-channels within the cutting or tool holder and deliver high-

pressure coolant jets precisely at the tool-chip interface, leading to a far improved cooling, lubrication, and chip evaluation. The issues of thermal instability, insufficient cutting force, and built-up edge formation observed in hard-to-machine alloys are significantly minimized with internal cooling. Especially in high-speed milling, internal cooling has become essential as it demonstrates strong advantages by effectively dissipating heat and maintaining tool performance and surface integrity [4]. High-pressure cooling (HPC) has also been developed to mitigate the issues encountered in the traditional flood methods, but it still suffers from the disturbance in tool rotation and inaccessible cutting zones [19]. Hence, the internal cooling system has proven to be a more robust and industrially applicable alternative as it ensures a consistent and disturbance-free coolant jet [14].

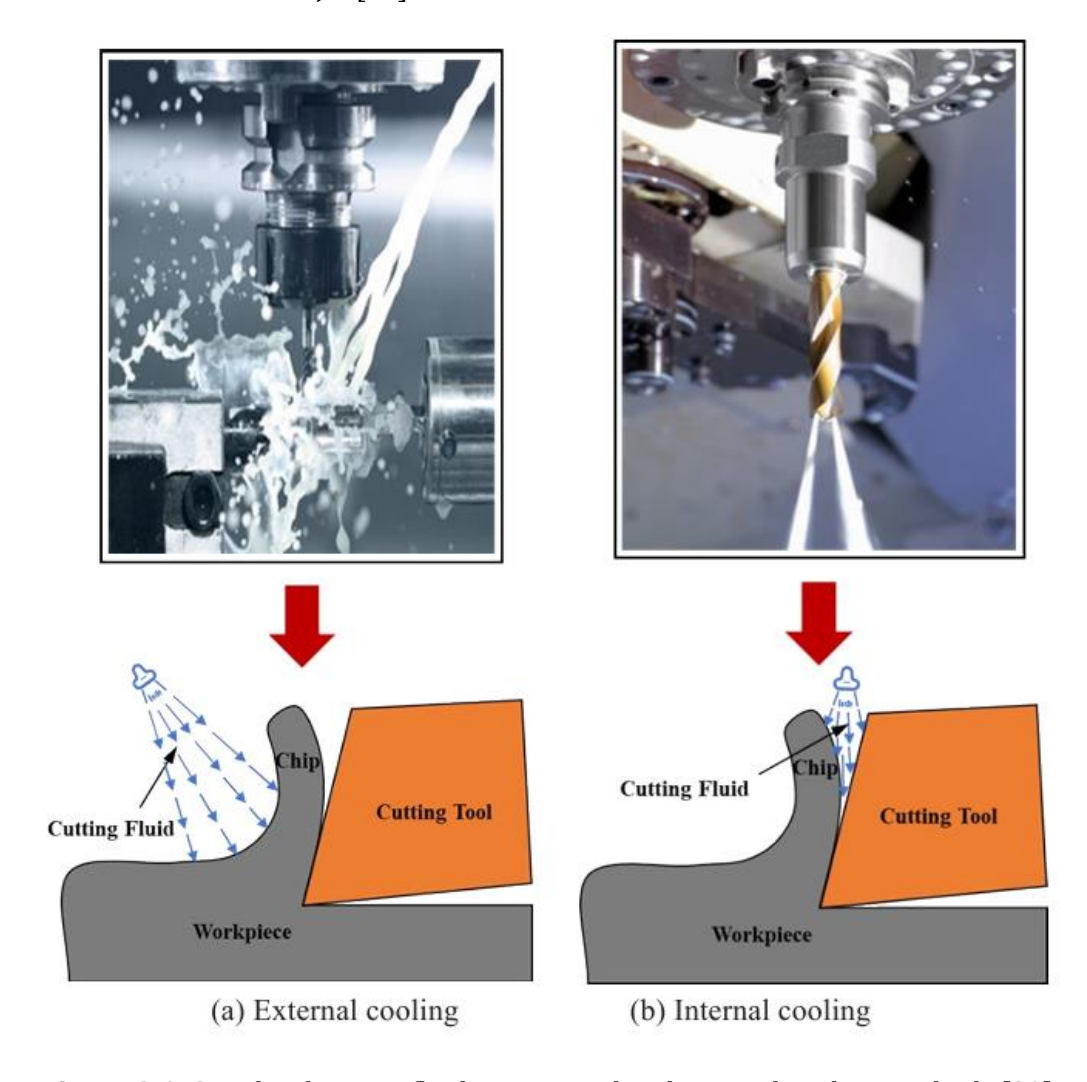


Figure 2.1: Supply of cutting fluids in external and internal cooling methods [20].

Research has been conducted by integrating high-pressure cooling (HPC) and internal cooling technology. The cutting experiment conducted by Polvorosa et al. [21] on Inconel 718 and Waspaloy involved using coolant pressure up to 80 bar. Their results showed

that compared to a low pressure of 6 bar, HPC greatly reduced the flank wear in both materials and minimized adhesion wear in Inconel 718. Suárez et al. [22] did similar cutting tests and found that cooling on Haynes 282 at pressure under 80 bar results in 20% reduced cutting and feed forces compared to the conventional cooling. An experiment of Ti-6Al-4V using HPC was performed by Bermingham et al. [4], which showed a noticeable improvement in tool life and productivity over flood cooling. Courbon et al. [23] conducted a numerical study to investigate the effect of cutting fluid jets on machining. The study focused on the constant forces and thermal loads induced by the coolant jet and results showed that the coolant jet contributes to the reduction of cutting forces, chip radius, and tool-chip contact length, while also redistributing the contact pressure and temperature fields. These findings suggest that the directional control of coolant jets using internal channels along with optimized pressure, can substantially enhance the machining of superalloys.

In parallel, studies have focused on the development of intelligent design and the evaluation of internal cooling systems. Sun et al. [24] designed a smart cutting tool with internal cooling and temperature sensors usable for adaptive machining. They performed cutting tests on Al6063 in both dry conditions and wet conditions and found that internal cooling was able to effectively reduce the tool temperature. The concepts of efficiency ratio and specific efficiency ratio were introduced by Ferri et al. [25] during their study on internal cooling performance through microfluidic channels. The outcome demonstrated improvement of cooling efficiency with the decrease in cutting speed and feed rate.

The study by Peng et al. [26] involved machining of nickel-based superalloy with a pressurized internal cooling grinding wheel, which was able to achieve better heat transfer and enhanced surface quality in comparison to the flood methods. Both numerical and experimental research were conducted by Oezkaya et al. [27] to evaluate the internal cooling in Inconel 718 drilling. The results confirm the elimination of thermal dead zones and mitigation of tool wear under suitable coolant pressure. Qin et al. [28] made a comparison between internal and flood cooling in drilling Inconel 718 with nitride-coated tools and presented that the internal cooling was able to extend tool life by a factor of 2.05 while also reducing the thrust force. Vaporized internal cooling was employed during face milling experiments on AISI 316 by Wisley Sales et al. [29], which showed that with the increase of coolant flow, tool life and surface quality significantly improved. The outcomes from Sasahara et al.'s [30] study indicate that, while grinding carbon fiber reinforced plastic (CFRP), internal cooling could suppress

loading and contribute to a superior surface finish. These studies highlight the vital role of internal cooling in the machining of superalloys and advanced materials. There is a growing industrial demand for efficient and sustainable machining of superalloys which complements the need for more detailed investigation into internal cooling strategies during end milling to better enhance cutting efficiency, tool life, and surface integrity.

2.2. Computational Fluid Dynamics in Machining

In recent years, Computational Fluid Dynamics (CFD) has emerged as a powerful tool in machining research. The coolant flow behavior in regions that are otherwise inaccessible during cutting operations can be accurately predicted and visualized by the application of CFD. In processes such as milling, where coolants play a vital role in controlling heat, maintaining lubrication, and evacuating chips, the direct observation of the coolant distribution near the cutting zone is very challenging as there are often visual obstructions, extreme temperatures, and intense mechanical loading associated. Typical experimental approaches, including thermocouple embedding and infrared imaging [31], most of the time are unable to provide desired insights on the coolant flow behavior due to the constraints in accessibility and resolution. CFD in this context poses as a viable option as it offers reliable modeling of fluid flow, heat transfer and tool-fluid interactions under conditions that closely resemble real machining phenomena [32].

Several studies have explored the use of CFD to investigate both fluid flow patterns and thermal characteristics of machining. Works published by Johns et al. [7] and Fallenstein & Aurich [5] presented the effective implication of CFD in drilling to optimize coolant distribution and improve thermal management, depicted in Figure 2.2. Their research contained insights into the design of the cooling channel, flow uniformity, and reduction of the tool wear. Uhlmann et al. [6] developed more advanced models that integrated coolant flow prediction with thermal behavior. The approach was particularly interesting for the intermittent cutting processes like milling, as it worked the unique challenges of rapid temperature fluctuations and periodic tool engagement. Bräunig et al.[33] developed a CFD model to investigate the multi-phase coolant flow around cutting tools, highlighting how coolant distribution can impact thermal behavior and machining precision, as shown in Figure 2.3. Validated through experimental tests, their study emphasizes the need for accurate coolant flow modeling to achieve improved tool cooling and minimized thermal distortion, especially in high-speed machining. Naumann

et al. [34] implemented CFD simulations to make a comparison among cooling methods in machining. The outcomes indicated water-based cooling to be most effective in reducing tool temperature and machining performance.

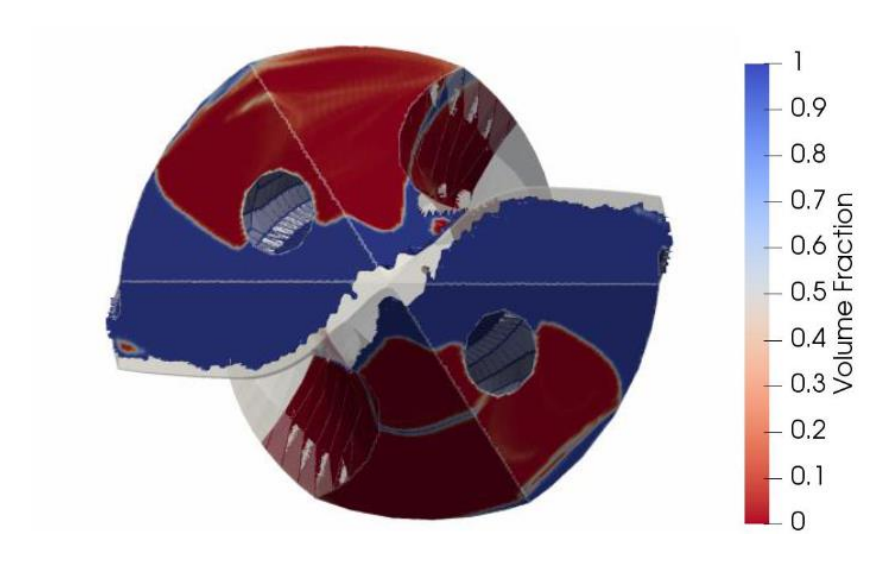


Figure 2.2 : Coolant volume fraction in the drilling simulation developed by Johns et al. [7].

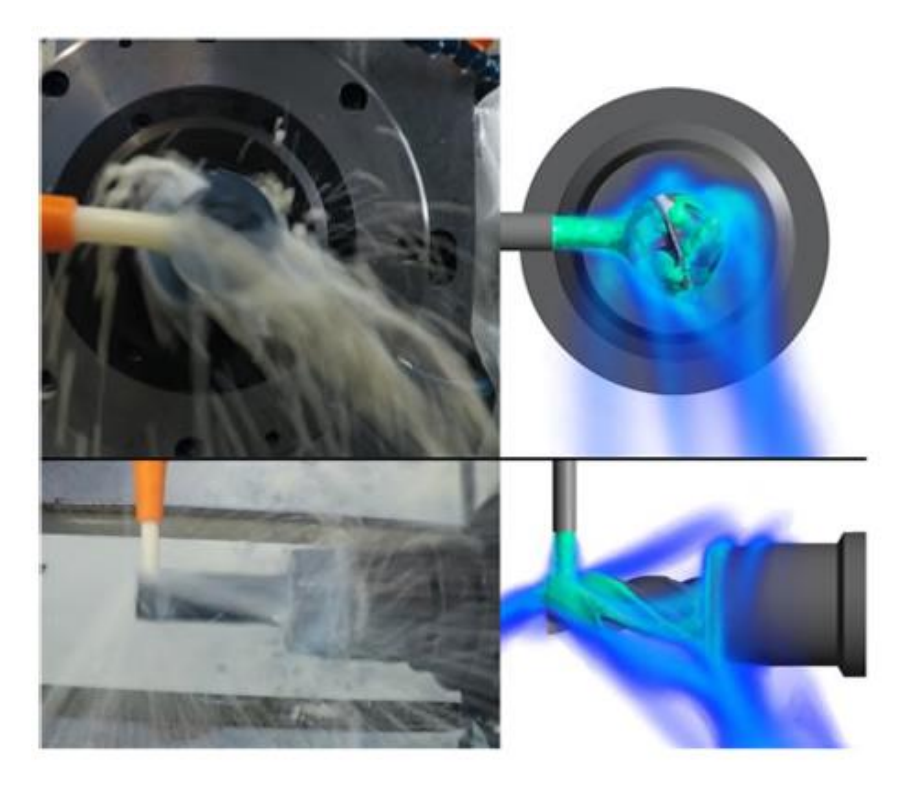


Figure 2.3 : Comparison of experimental and simulated coolant flow in the study by Bräunig et al. [33].

The performance of external jet cooling has also been evaluated by CFD. A fluid-structure-interaction (FSI) simulation was carried out by Brier et al. [35] to investigate the effects of thermal tool elongation during machining. Their approach took into account CFD and structural simulations to model and correct thermal deformations caused by coolant flow and cutting forces. The work signified the critical role coolant delivery systems play in enhancing thermal distribution and machining accuracy. Similarly, Brier et al. [36] also worked on a CFD model to assess convective heat transfer during jet cooling in milling, indicated by Figure 2.4. The outcomes indicated the importance of optimized coolant flow in achieving improved thermal management and machining precision. The milling cutter model developed by Najiha et al. [37] indicated that due to the geometrical barrier, coolant jets often do not reach the cutting edge. Their further work involving three symmetrically placed nozzles demonstrated improved coolant distribution; however, these models did not incorporate the factors of workpiece or chips [38].

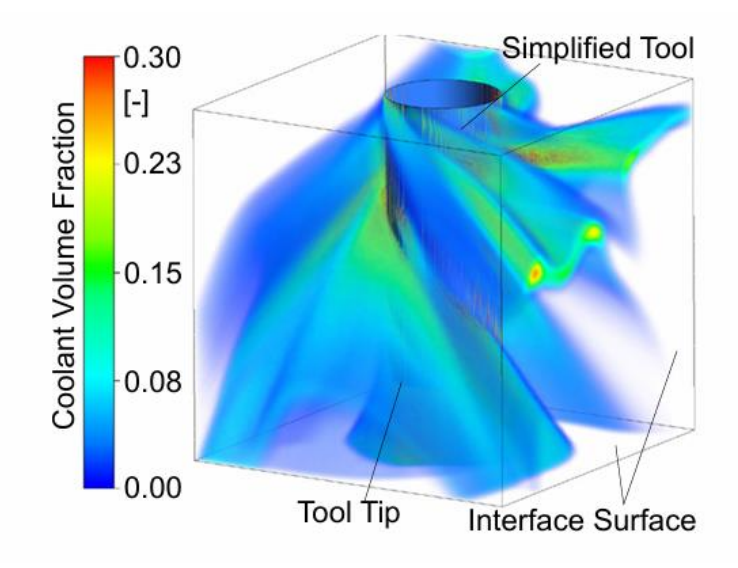


Figure 2.4: Volume fraction of coolant Flow noted in the study by Brier et al.[36].

Tool rotation adds a substantial level of complexity in coolant flow dynamics. Duchosal et al. [39] and Oezkaya et al. [27] emphasized it and highlighted the impact of high spindle speeds. It was presented that with high spindle speeds, centrifugal forces are generated, which can significantly alter the flow trajectory. If the coolant was supplied at a lower pressure, the flow jets might get deflected away and not reach the desired region of the cutting zone. It was interesting to note that within certain speed ranges, rotation could actually assist in directional cooling by enhancing the horizontal velocity component, which could result in contributing to the chip evacuation.

Oezkaya et al. [27] conducted simulations on internal cooling and observed the formation of cooling dead zones near the cutting edge, which they mentioned could not be eliminated by varying coolant pressure or modifying channel diameter. Later work by Biermann and Oezkaya[40], however, showcased how redesigning the outlet geometry internal channels could contribute to better flow focus and enhanced velocities (Figure 2.5), and in mitigating these dead zones. In separate works, Zachert et al. [41] and Peng et al.[42] reported non-uniform coolant velocity and pressure distribution in conventional tools, showcased in Figure 2.6 and Figure 2.7. Their investigation revealed that the reason was flow separation and high turbulence caused by the sharp intersections and poor surface finish of the channels.

Furthermore, cutting speed and fluid velocity ratios have been studied in relation to the Leidenfrost effect. Due to the Leidenfrost effect, coolants tend to vaporize prematurely at high surface temperatures. CFD results [43] depicted that when the coolant is directed at a velocity less than twice the cutting speed, the access to the tool-chip becomes increasingly difficult. At extreme spindle rotation, additional challenges occur, such as fluid cavitation and loss of contact, leading to further degradation of cooling performance.

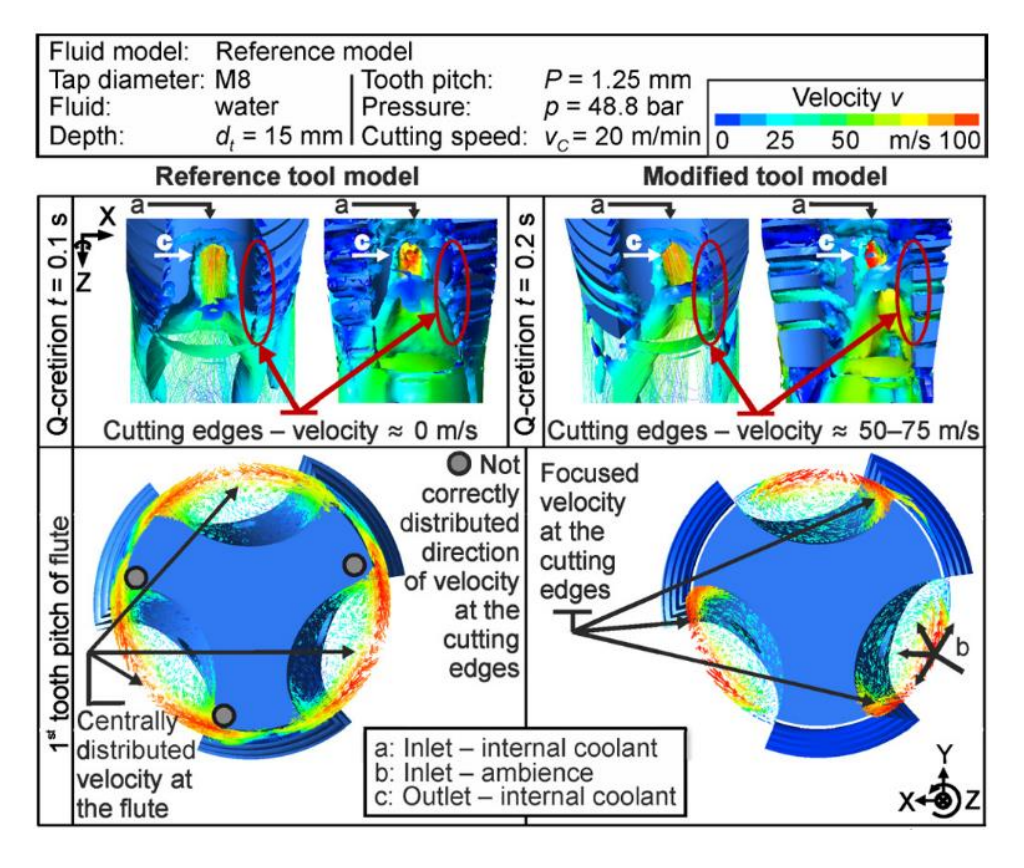


Figure 2.5 : Comparison of fluid volume distribution from the study of Biermann and Oezkaya [40].

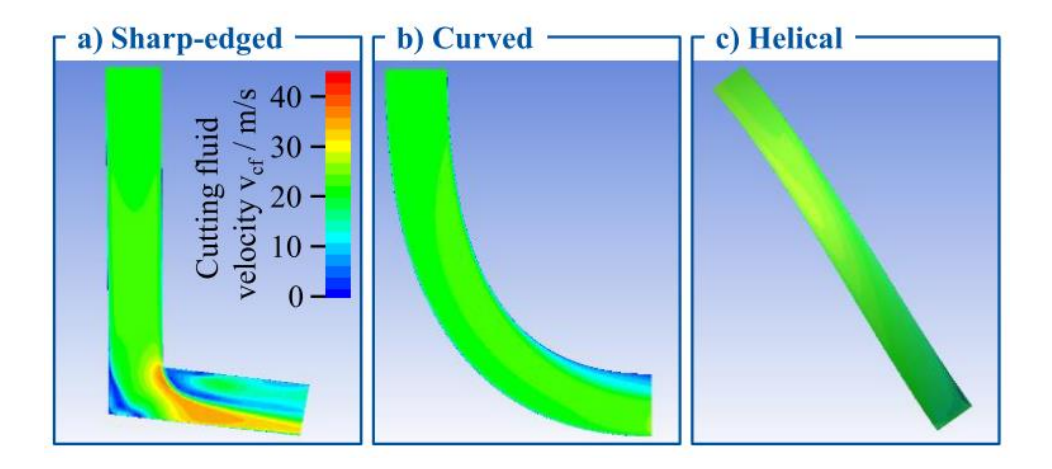


Figure 2.6 : Comparison of fluid velocity distribution from the study of Zachert et al. [41].

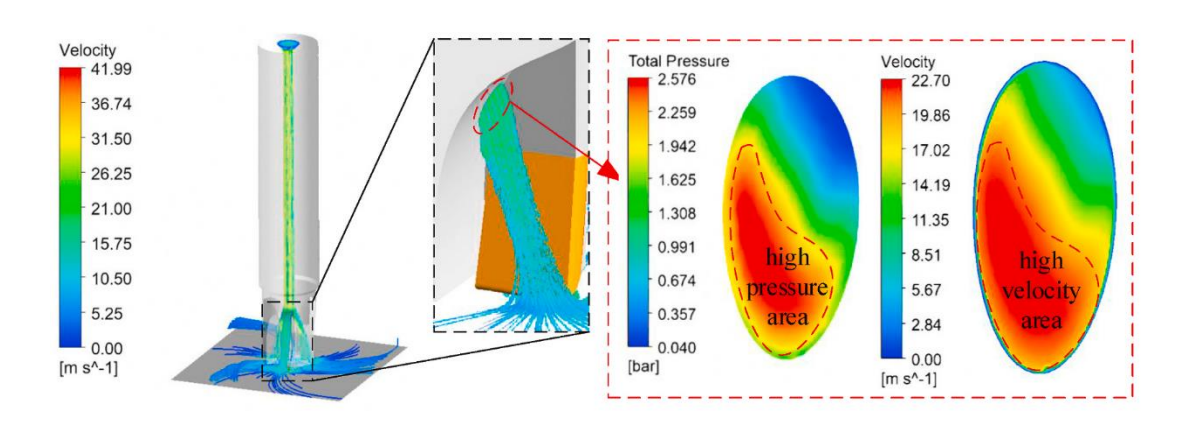


Figure 2.7 : Streamline of cutting fluid, outlet pressure and velocity distribution as reported by Peng et al.[42].

Despite the potential the practical implementation of CFD remains a challenge because of a number of technical limitations. The combination of complex cutting tool geometries, rotating motion, and coolant tribology makes it complicated to accurately realize the boundary conditions and generate high-quality mesh. It is also essential that a compatible turbulence model is applied, particularly for the cases of simulation of flows with rotational components and thermal gradients. Generally most models utilize k- ϵ or shear stress transport (SST) models but to achieve precise and reliable results, finer meshing near boundary layers and the correct definition of inlet and outlet conditions are often needed.

Three-dimensional CFD simulations are generally preferred as they are able to simulate the full interaction between coolant flow and tool geometry, although they demand significant computational power to resolve fine-scale calculations in dense meshes. 3D modeling enables the feature of vortical structures, a characteristic closely related to the rotating system and has a significant impact on turbulence intensity and energy dissipation. To identify and evaluate these flow structures techniques such as q-criterion and λ^2 -method are most frequently implemented [44].

Given the challenges observed in both experimental and numerical modeling, CFD has become a commonly used tool for optimizing tool design, designing cooling channels, and planning advanced machining. However, the successful application relies on a well-constructed model, careful validation, and inclusion of realistic factors such as tool rotation, coolant properties, and thermal loads. CFD models can be leveraged to their maximum possible limit by integrating multi-physics models that simultaneously consider fluid flow, heat transfer, and structural deformation for applications involving internal cooling in rotating milling tools.

2.3. Internal Cooling Channel Design and Optimization

Achieving an effective system of internal coolant supply requires careful consideration of geometry and functional design that would ensure that the coolant reaches critical cutting zones without a significant energy loss. This is impacted by multiple interrelated factors, including the shape and layout of cooling channels, their cross-sectional design and manufacturing methods, coolant's volumetric flow, and nozzle configuration. Analysis of these parameters is extremely challenging with experimental rigs, as accurate measurement is quite difficult to obtain. In this regard, CFD proves to be an essential tool that can qualitatively evaluate and describe the flow of the field. Hence, CFD simulations have become the pioneering tool to refine these features to enhance cooling and lubrication during machining.

In order to maximize the benefits of internal cooling, the key concerns are on coolant supply pressure and internal channel geometry to ensure the uniform coolant supply to the tool-chip or tool-workpiece interface. Minimizing fluid mechanical loss, particularly the pressure drop, is considered an important objective here, as otherwise this can significantly diminish cooling performance. It was noted that while straight channels in general fulfill this criterion and offer very good flow efficiency, their limitation lies in reaching the intricate cutting zone. Therefore, branched channels are in more use compared to the straight channels, although typical drilling of branched channels adds complexities such as sharp intersections that disrupt the flow and might contribute to

the adverse effects of backflow, reduced outlet pressure, diminished jet velocity and occasional cavitation [20].

CFD simulations have proposed the introduction of transition radii at intersections to mitigate this issue. The study by Kelliger et al. [45] indicated that with the addition of a 5 mm transition radius, volumetric flow rates saw a significant rise of 27 % compared to the channels with only sharp-edge intersections (Figure 2.8). It was also reported that with the further increase of radius, the velocity distribution got better. Zachert et al. [41] conducted similar research, where their design included a 30-degree radius in place of the sharp corner, and resulted in 23% more volumetric flow. These findings point out the need for smooth transitions to obtain an enhanced flow efficiency and uniformity.

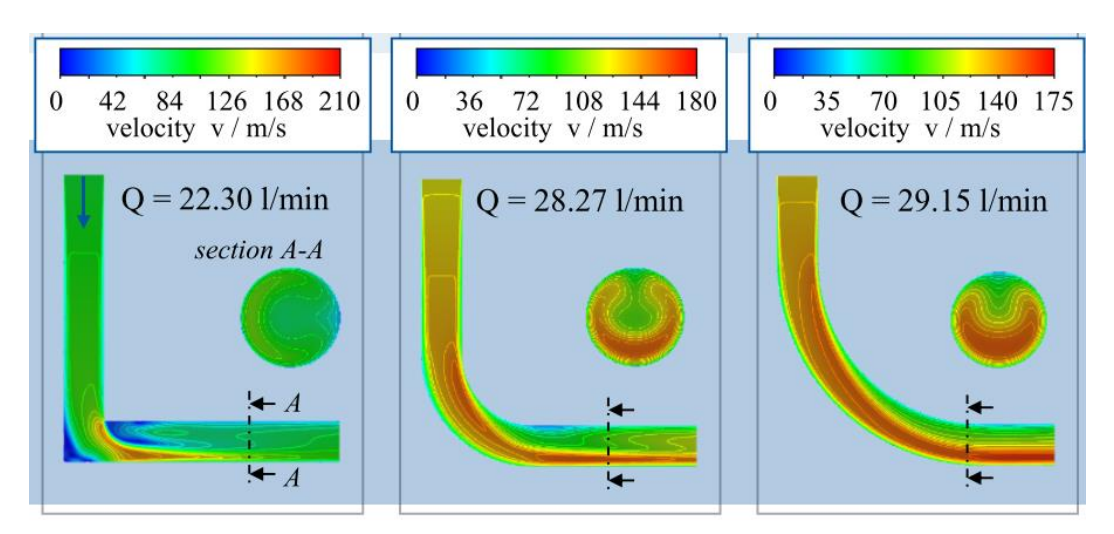


Figure 2.8 : Velocity profiles from CFD analysis of internal cooling channels with varying transition radii, based on the findings of Kelliger et al. [45].

The cross-sectional shape and size of the internal channels have a direct impact on the cooling capacity and the tool's structural stability. Circular cross-sections are widely used in most applications as they often provide the benefits in terms of favorable hydraulic radius, pressure resistance, and minimized stress concentration. However, studies suggest that for additively manufactured tools, this option might not be ideal. As Kelliger et al. [45] reported, better performance of horizontally built triangular cross-sections was observed when applied in a similar area. Nonetheless, it is still quite complicated to incorporate such geometries into the curved paths without overhangs; there is a high risk associated with the possibility of generating poor orientation during printing.

In addition, there is a concern of surface roughness inside the channels that can hinder the flow. Kugaevskii et al. [46] showed that tools manufactured by selective laser melting

(SLM) can achieve mechanical strength compared to the conventional tools; there might be a need for post-processing, such as abrasive flow machining, to function properly.

The volumetric flux of coolant is an important parameter when evaluating cooling performance and it is closely tied to the channel cross-sectional area. Klocke et al. [47] and Oezkaya et al. [27] confirm the benefits of higher flux to improve heat removal, chip evacuation, and surface finish. However, there is a potential barrier that compromises the tool stiffness. Therefore, there should be a trade-off between thermal efficiency and mechanical integrity, and a right balance needs to be employed, particularly when dealing with heat-sensitive materials like Inconel 718.

The nozzle design of internal cooling systems involves three key aspects, posture, shape, and number (Figure 2.9) [20]. The nozzle posture refers to its position and orientation, which dictates whether the coolant should be directed at the tool-chip or tool-workpiece interface [48]. When the coolant jet targets the tool-chip interface, the cutting temperature reduces so as the cutting force. But problems arise in the form of crater wear produced by the direct impact on the rake face, which is associated with high-pressure coolant flows resulting in high impact velocities. On the other hand, aiming coolant flow at the tool-workpiece interface is useful in obtaining a better surface finish as a lubricating layer is produced at the interface. The most effective cooling configuration utilizes the benefits of both modes, though it is very complicated to implement due to the structural limitations [49], [50].

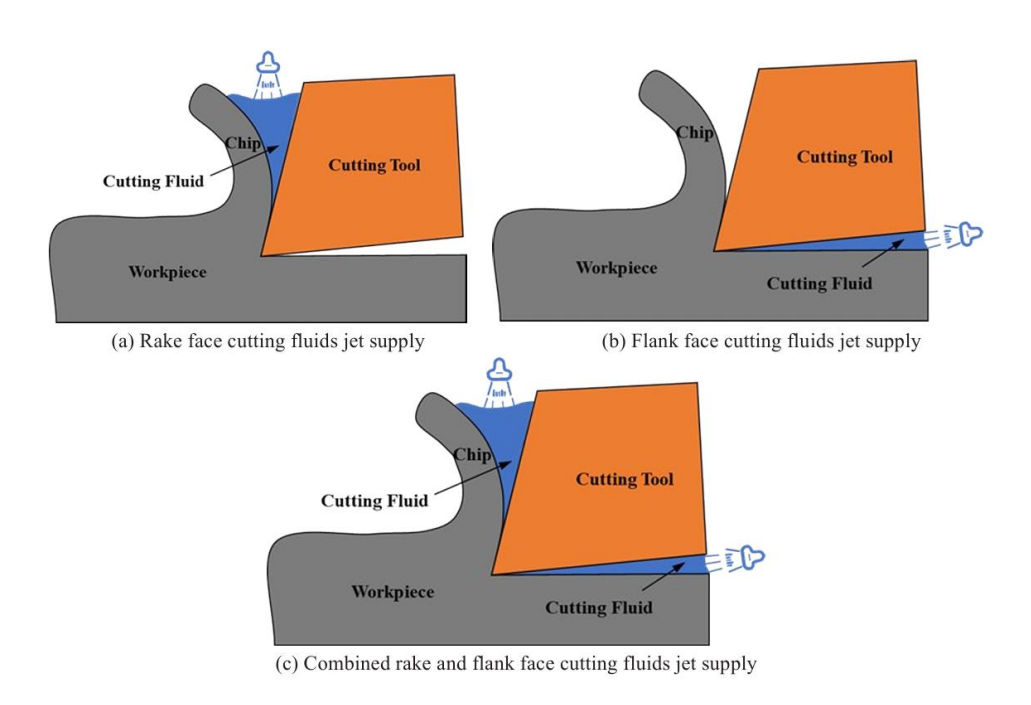


Figure 2.9: Cutting fluid supply at different nozzle orientations [20].

There are still no standardized guidelines or universally accepted criteria for optimizing nozzle orientation. Most designs are developed through trial and error, leading to a great variety of constructions [51]. Nonetheless, it is well established that the closer the nozzle is positioned to the cutting edge, the better the coolant focus and energy delivery [45]. A similar principle is applicable to nozzle shape also. The more narrow and concentrated the jet are minimal is the fluid dispersion. Regarding the nozzle number, the general recommendation is to employ at least one nozzle at the rake face of each cutting edge. To obtain enhanced performance, multi-nozzle configurations are implemented to cool both rake and flank faces, enabling much better lubrication and thermal control [20].

2.4. Research Gap and Summary

The reviewed literature provides valuable insight into how CFD can be applied to simulate coolant flow and optimize cooling systems in machining, particularly for the instances in end milling. However, there are still gaps that need to be worked upon to gain a complete understanding of coolant flow dynamics and their implications on machining performance.

In spite of substantial research on CFD simulations, much remains unexplored regarding coolant behavior in the dynamic and complex context of end milling. Studies such as those by Bräunig et al. [33] and Naumann et al. [34] emphasized the need for accurate models to capture the interaction between coolant and rotating tools. However, there is still a lack of experimental validation under real-world conditions. This gap calls for a more reliable simulation approach that considers high-speed cutting, coolant flow rate, and changes in geometry.

While CFD is an established and powerful tool for modeling coolant behavior, it has often been used independently without following a systematic approach. To get a comprehensive evaluation of the interacting parameters, it is required that the simulations be performed in a systematic manner. The Design of Experiments (DOE) concept provides a structured framework through which multiple factors affecting coolant performance can be evaluated simultaneously. In fact, there is great potential in integrating CFD with DOE to optimize the internal cooling system. This CFD-DOE approach can be useful in identifying the key parameters that significantly impact cooling efficiency.

In the context of optimizing internal cooling systems in end milling, there still exists a significant gap. Several studies, including Kelliger et al. [45], have focused on redesigning channel geometry and reducing pressure loss, but there is still a lack of applicable solutions that can integrate these designs with the real-time machining environment. Hence, a comprehensive multi-physics simulation is required that combines tool design, workpiece geometry, and machining and lubrication phenomena to better understand the impact of coolant flow in machining.

Many existing models have overlooked tool-specific variations that can significantly impact coolant flow dynamics. Brier et al. [36] mentioned that while surrogate models can be useful in addressing this issue, they still need to be redefined before application across different tool types and machining environments. This highlights the requirement for a generalized model that can be relied upon to predict coolant performance for diverse tool designs and cutting conditions, replicating real-world milling scenarios.

From the existing literature, it is clear that CFD modeling has high significance in optimizing internal coolant flow in end milling, although several research gaps still persist. The gaps can be summarized in terms of limited understanding of coolant behavior, the lack of an integrated CFD-DOE approach and challenges in implementing CFD models in actual machining. Addressing these gaps and resolving them is crucial for advancing cooling design and achieving high-performance milling.

Chapter 3

Methodology

3.1. Research Design

In this study, a Computational Fluid Dynamics (CFD) model was developed to conduct the simulation of the coolant flow in end mill operations with an internal coolant supply system. The primary focus was to evaluate the flow morphology and to investigate the supply of coolant in the desired regions of the cutting zone. Particularly in dynamic machining and coolant conditions, it was important to monitor the coolant behavior. Additionally, the research intended to compare the variation of workpieces that was impacting the cooling performance. With the implication of the Design of Experiment (DOE), the goal was to obtain a numerical model that can be implemented in a broader perspective and would be helpful in the optimization of the coolant performance in machining. In order to ensure the accuracy and reliability of the CFD model, the simulation results were validated through surrogate experiments. Experiments were conducted in the workshop, using similar operating conditions as the CFD simulations, and the coolant flow behavior was monitored subsequently. By comparing the simulations with experimental observations, the study made sure the reliability of the developed CFD model to serve as a strong tool for future investigations into coolant flow dynamics.

The methodology employed in this study is illustrated in the flowchart in Figure 3.1. At first, a comprehensive CFD was constructed that includes the tool design, workpiece geometry, coolant system, and boundary conditions representing the operating phenomena. Then, with the help of DOE, key input parameters such as workpiece geometry, coolant type, tool rotation, and coolant flow rate were structured to be implemented in the model. After that, simulations were performed following the organization of the DOE, and outcomes were noted down. Next, real-life cooling was performed, replicating the constraints applied in a surrogated CFD model, and a comparison of coolant flow behavior was made. Finally, results from the actual CFD model were analyzed to obtain an insight into the optimization of coolant performance.

Development of the CFD model

- Define tool geometry, workpiece, and coolant system
- · Set boundary conditions and mesh resolution
- Choose turbulence model and solver settings

Design of Experiment (DOE)

- · Identify key input parameters
- Define levels for each parameter
- Structure experiments to explore key parameter effects

Execution of Simulation

- Monitor convergence and flow field stability
- Export velocity, turbulence, and volume fraction data

Experimental Comparison

- Conduct milling experiments under simulation conditions
- Compare experimental results with CFD simulations

Analysis and Optimization

- Analyze results
- Optimize coolant parameters

Figure 3.1: Methodology flowchart for CFD analysis and coolant optimization.

3.2. CFD Model Development

To analyze the internal coolant flow behavior in milling, a compatible tool design was needed. For this study, a simplified tool geometry was developed on the basis of the commercial Harvi Ultra 8X end mill from Kennametal, as presented in Table 3.1 and Figure 3.2 [52]. In CFD software environment, it was essential that complexity is reduced as much as possible while maintaining functional accuracy to fully optimize the computational power. In the developed tool, the original coolant nozzles were replaced with evenly placed cylindrical holes along the tool's circumference. The approach was sent to Kennametal, and their feedback confirmed that the simplification was acceptable for simulation purposes.

The tool design incorporated a total of 24 holes. There were four large holes, each 2 mm in diameter, at the end of the tool and twenty small holes, each 1.4 mm in diameter, equally distributed above them. With the selected configuration, a consistent and balanced coolant distribution was expected to be achieved as all holes were uniformly spaced along the flutes. The geometry was created in SolidWorks. The tool length and diameter were 98 mm and 63 mm, respectively, retaining the dimensions of the commercial tool. It includes 4 flutes completing one full revolution along the tool's length. After the construction, the final geometry was exported for meshing and CFD simulation.

Parameter	Specification
Tool Type	Simplified Harvi Ultra 8X
Total Number of Coolant Holes	24
Large Coolant Channels	4 holes, 2 mm diameter, near tool end
Small Coolant Channels	20 holes, 1.4 mm diameter, above large holes
Hole Distribution	Evenly spaced along flutes
Number of Flutes	4 (helical, one full revolution)
Tool Length	98 mm
Tool Diameter	63 mm
Modeling Software	SolidWorks

Table 3.1: Geometrical specifications of the modeled end mill tool.

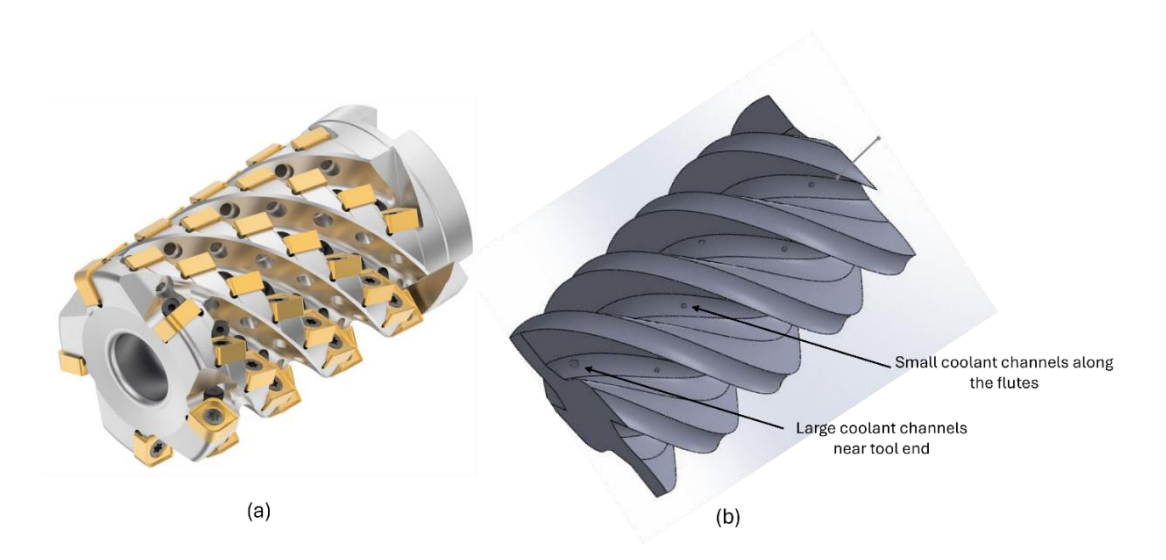


Figure 3.2 : (a) Original Harvi Ultra 8X tool [52] and (b) simplified tool geometry with coolant channels.

For the current work, two distinct workpiece profiles, flat and curved, were considered. The flat workpiece was selected to simulate a typical planar surface, widely encountered in standard machining. On the other hand, curved workpiece replicated complex contoured surfaces found in components such as turbine blades or biomedical components. This selection was particularly interesting to observe the influence of curvature on flow behavior. The inclusion of both workpiece shapes ensured that the study addressed practical considerations of both standard and advanced manufacturing applications.

The components of the model were imported and defined in ANSYS Design Modeler. The system includes a simulation domain of 200 mm × 200 mm × 200 mm, inside which the milling tool, the workpiece, and a plate are placed to replicate the real-life machining, indicated in Figure 3.3.

Meshing was done in ANSYS Meshing by utilizing a CFD-oriented approach in order to correctly capture complex flow features within the internal coolant system, shown in Figure 3.4. To obtain an effective mesh, a linear element order was used, and CFD physics preference was implemented with solver compatibility enabled for CFX. For the entire domain, a global element size of 0.01 m was applied uniformly. A local face sizing was introduced at the coolant channel inlet, refining the mesh to 0.0005 m. It was necessary to achieve an enhanced resolution in this critical flow region. The domain includes flutes and internal channels on the tool, and hence, curvature and proximity-based refinement were activated to improve the mesh conformity. In addition, mesh quality control was turned on with medium smoothing and a target skewness of 0.9.

The final mesh statistics, as presented in Table 3.2, included approximately 199,000 nodes and 930,000 elements, which ensured a balance between numerical precision and computational cost. Before setting the solver settings, key mesh metrics such as element quality and minimum edge length were observed, and they were found to be within the acceptable standards of CFD analysis.

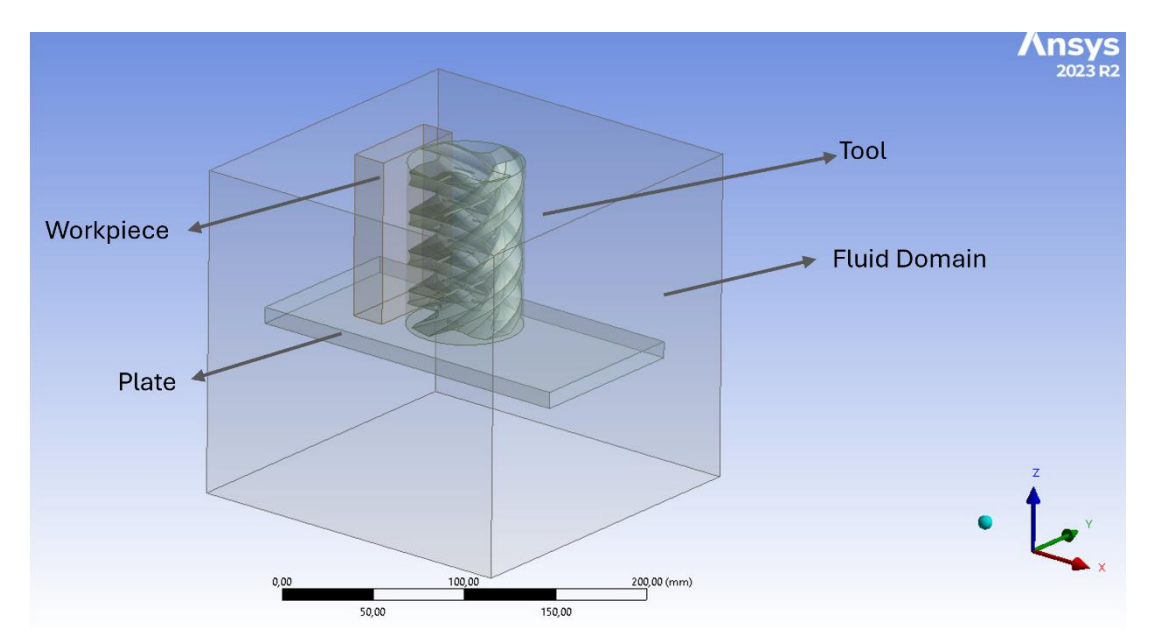


Figure 3.3 : CFD model setup in ANSYS showing the fluid domain (200 × 200 × 200 mm) containing the milling tool, workpiece, and mounting plate.

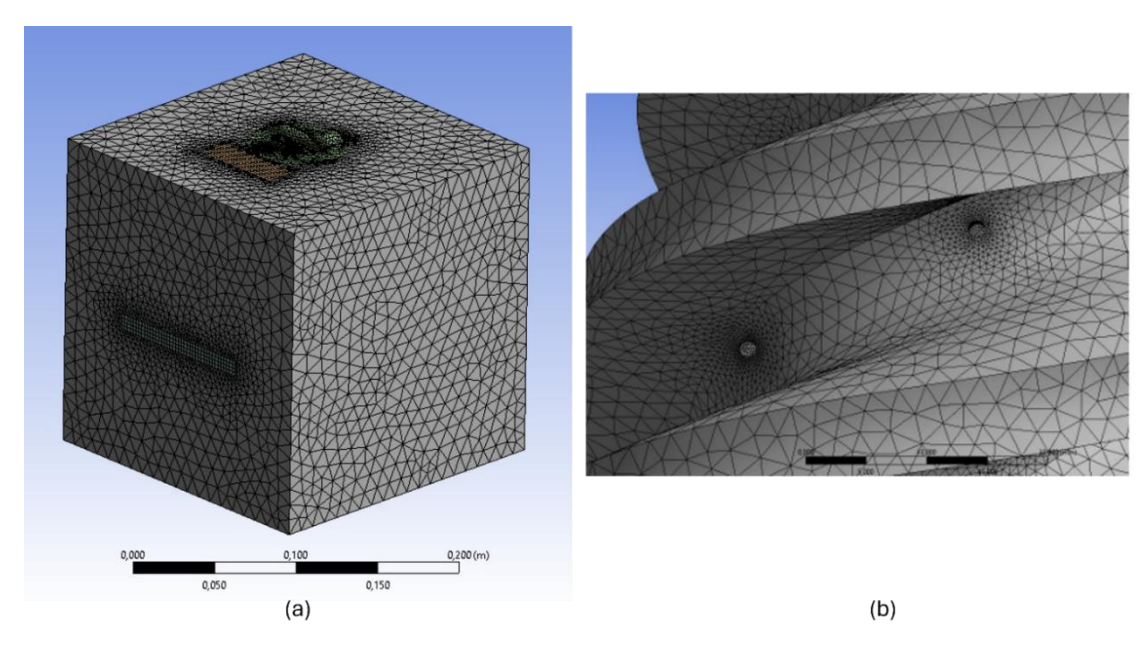


Figure 3.4: (a) Global mesh view and (b) Localized refinement near coolant inlets.

Parameter	Value / Setting
Physics Preference	CFD
Solver Preference	CFX
Element Order	Linear
Global Element Size	0.0100 m
Face Sizing (Coolant Inlet)	0.0005 m
Curvature and Proximity Capture	Enabled
Smoothing	Medium
Target Skewness	0.9 (Default)
Nodes	199,394
Elements	930,475

Table 3.2 : CFD meshing parameters and settings.

ANSYS CFX, as the CFD solver, was utilized to perform the simulation of internal coolant flow. The analysis was carried out under the approximation that the system is in a steady, incompressible, and isothermal state. It was assumed that no heat transfer, radiation, or phase change was occurring as the study explicitly focused on the flow dynamics.

The CFD simulation is rooted in the numerical solution of the Navier–Stokes equations, which explain the fundamental laws governing fluid motion [53], [54]. This covers mathematical expressions such as the continuity equation (3.1) and the momentum equation (3.2). Because the current study dealt solely with the hydrodynamic aspects of the coolant flow, thermal and compressibility effects were disregarded, and the energy equation was not involved.

$$\nabla v = \frac{\partial v_x}{\partial x} + \frac{\partial v_y}{\partial y} + \frac{\partial v_z}{\partial z}$$
3.1

$$\rho \left(\frac{\partial v}{\partial t} + (v \cdot \nabla) v \right) = f - \nabla p + \eta \cdot \Delta v$$
 3.2

Here, symbols are denoted as ρ (density), f (volume force), t (time), p (pressure), ν (velocity), η (dynamic viscosity), and x, y, z (spatial directions).

To account for the turbulence, the Shear Stress Transport (SST) formulation of the k- ω model was employed. The model solves two additional transport equations for turbulent kinetic energy (k) and specific dissipation rate (ω). It was expected that with these settings, the simulation would accurately capture near-wall effects and rotational flow behavior.

The simulation domain as depicted in Figure 3.5, consisted of a rotating fluid region that included the milling tool, a static fluid region surrounding it, and adjacent solid regions to specify the tool, workpiece, and mounting plate. Two immiscible fluids, such as the coolant and air, were defined as continuous fluids in the fluid domains. ANSYS CFX Material Library was utilized to assign material properties. The domain was set as buoyant, and gravity was applied in the global z direction to account for gravity-influenced effects.

The rotating domain was applied with angular velocity about the global z-axis to incorporate the tool rotation. At the fluid-fluid interface, the Frozen Rotor model was assigned to couple the rotating and stationary domains. This allowed a steady-state approximation of relative motion in place of computationally demanding transient computation. Throughout the simulation, the geometry stayed rigid; hence, the mesh deformation option was disabled.

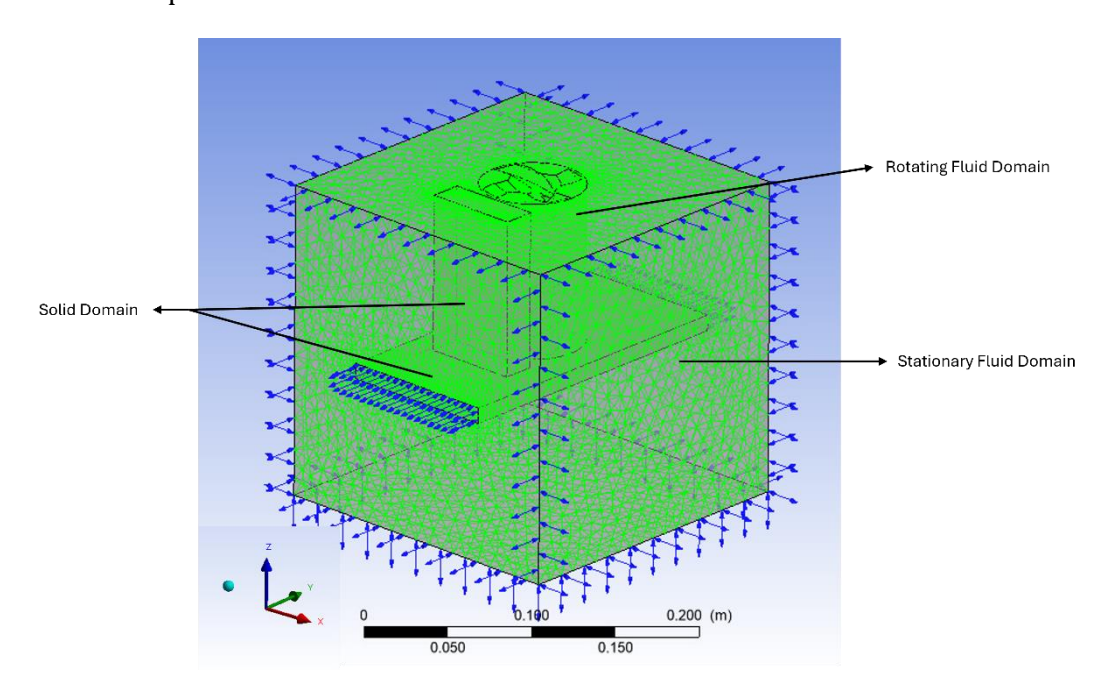


Figure 3.5 : Domain setup for CFD simulation.

Table 3.3 summarizes the boundary conditions applied in the simulation. There was a mass flow inlet to introduce the coolant, a pressure opening, and wall conditions for both the rotating tool and the enclosed surfaces. It was necessary to specify volume fractions of air and coolant to define phase dominance at the respective boundaries. Additionally, wall settings were input based on the domain configuration.

Boundary	Туре	Specification
Coolant Inlets	Mass flow inlet	Flow rate (kg/s) and coolant volume fraction
		set to 1.0
Opening	Pressure Opening	Pressure set to 0 Pa (gauge) and air volume
		fraction set to 1.0
Tool Wall	Wall	Rotating wall motion with default no-slip
		condition
Enclosure Walls	Wall	Stationary wall with default no-slip condition

Table 3.3: Summary of boundary conditions used in the CFD simulation.

The solver settings were configured in such a way that they could ensure numerical stability, efficient convergence, and accurate representation of the flow patterns of the coolant. To account for the stability and accuracy, a high-resolution advection scheme and a first-order turbulence numerical scheme were applied. Root mean square (RMS) residuals were implemented to track the convergence, with a target threshold of 1.0×10^{-4} . In addition, conservative automatic timescale was selected with a timescale factor of 0.5. This selection smoothens the balance between stability and convergence rate. A depiction of solver settings is shown in Table 3.4 .

Simulation Type	Steady-State
Advection Scheme	High Resolution
Turbulence Numerics	First Order
Residual Target (RMS)	1.0×10^{-4}
Timescale Control	Auto (Conservative)
Timescale Factor	0.5
Turbulence Intensity	Medium (5%)

Table 3.4 : Solver control settings.

After each CFD simulation, quantitative flow parameters relevant to coolant delivery performance were analyzed in ANSYS CFX-Post. A fixed reference location was created within the computational domain for the calculation as presented in Figure 3.6, which ensured consistency in the comparability of all simulated cases.

The reference location was located at the YZ-plane, replicating the actual cutting-zone plane with a dimension of 200×10 mm rectangle. The position and the structure of the plane were oriented such that it would intersect the tool-workpiece engagement region, where the coolant interaction is most critical. The spatial dimension of the plane was kept the same for every simulation and was implemented as a basis for extracting all key performance indicators.

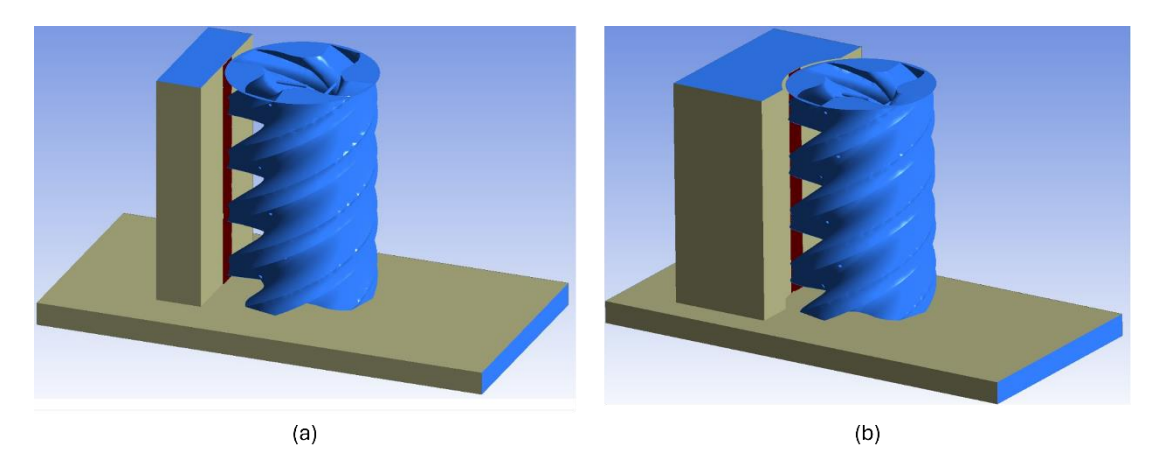


Figure 3.6 : Reference plane positioned at the cutting zone for coolant flow evaluation (a) Flat Workpiece (b) Curved Workpiece.

Four key parameters from the cutting-zone plane were obtained to evaluate the performance of the coolant delivery. The first one was average coolant velocity (m/s), measured as the area-weighted average of the coolant-phase velocity over the cutting-zone plate. It represented the mean jet speed in the target region and was closely linked with the coolant's penetration capability, convective heat removal, and chip evacuation efficiency. A higher average velocity would generally indicate the formation of a more energetic jet; however, excessively high velocities could initiate splashing or jet deflection. The average coolant volume fraction, defined by the area-weighted mean of the coolant phase volume fraction, indicated the proportion of the sampled plane occupied by the coolant compared to the air. Values approaching unity meant dense coolant coverage, while lower values suggested high affinity of air. A meaningful contact between the coolant and the cutting zone is required for efficient heat dissipation and lubrication. To account for the spatial extent of this, the parameter coolant coverage area fraction (%) was introduced. It was expressed as the percentage of the plane's surface

where the coolant volume fraction exceeded a threshold limit of 0.1. The threshold was implied to filter out the negligible amount of coolant formed as fine mist and to consider only the effective liquid impingement. The last parameter considered was the turbulence kinetic energy (m^2/s^2) , computed as the area-weighted mean of the coolant-phase turbulence kinetic energy. It provided a measure of the energy associated with velocity fluctuations. While elevated turbulence can be useful for mixing and convective heat transfer, after a certain limit, it might cause jet dispersion and directional instability.

3.3. Design of Experiments (DOE) Framework

In this study, the design of experiments (DOE) framework was implemented to organize the simulation run. The DOE method is widely used to systematically investigate the influence of key input parameters, and for the current research, it would be useful to understand each input's contribution to the output flow parameters [23]. The primary target was to evaluate the optimization in coolant performance with the help of response surface methodology (RSM), particularly through central composite design (CCD). This approach was able to effectively capture both linear and nonlinear effects across multiple variables.

The factors considered in this DOE were workpiece type, rotational speed, and coolant flow rate. Aside from these, variation of coolant type was also investigated, but it was not included in the DOE framework. Water and water-based semi-synthetic coolants are commonly applied in industrial machining for their cooling and lubricating properties, and the study considered both of them to observe any potential variation in the flow patterns. Physical properties of water and water-based semi-synthetic coolant utilized in the simulation are stated in Table 3.5.

Property	Water	water-based semi- synthetic coolants
Density [kg/m³]	997	990
Dynamic Viscosity [Pa·s]	8.899 x 10 ⁻⁴	1.26 x 10 ⁻³
Thermal Conductivity [W/(m·K)]	0.6069	0.533
Specific Heat [J/(kg·K)]	4181.7	4118.8

Table 3.5: Physical properties of water and water-based semi-synthetic coolant [55].

Factor levels in DOE are vital, and it was essential that the levels of each factor were chosen with established relevance. For the workpiece type, flat and curved were selected, as one accounts for the most typical milling while the other represents the milling in advanced applications. The rotational speed of the tool ranged from 250 RPM to 750 RPM in alignment with the tool specifications of HARVI™ Ultra 8X [52]. The lower speed of 250 RPM is representative of roughing on the other hand, the higher speed of 750 RPM is indicative of finishing. From the performance curve of the HARVI™ Ultra 8X tool as presented in Figure 3.7, the lower and higher values of 20 l/min and 30 l/min for the coolant flow rate were chosen [56]. Though at the higher flow rate up to 30 l/min, the cooling is enhanced, it comes with the cost of higher energy consumption. Therefore, a considerable range of flow rates was required to mimic the real-world machining conditions.

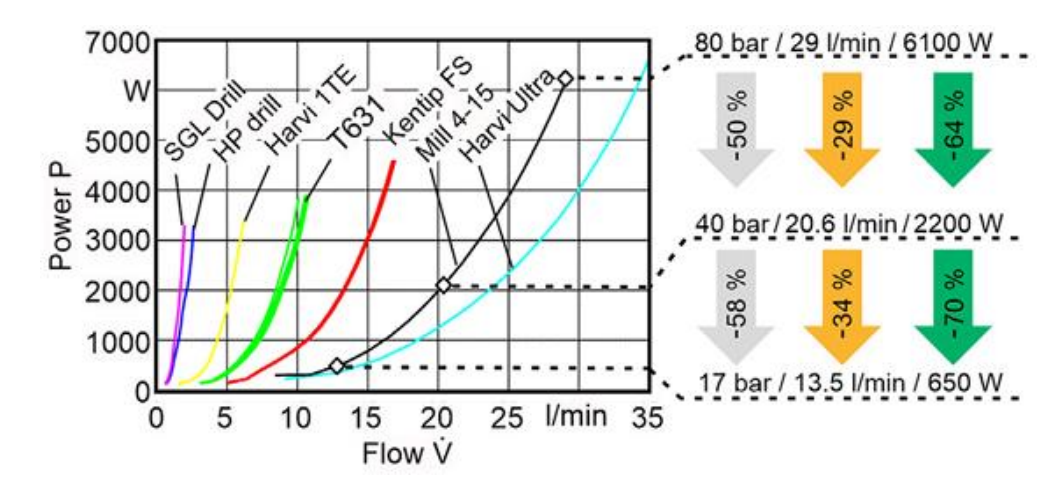


Figure 3.7 : Power consumption versus coolant flow rate for various milling tools, highlighting the HARVI™ Ultra 8X [56].

Using the CCD design in Minitab, a total of 26 simulations were planned, 13 simulation runs for each workpiece type. The implication of CCD design facilitated the evaluation of both main effects and interaction effects, providing a comprehensive insight into both linear and nonlinear effects on coolant behavior. DOE factors and levels are noted down in Table 3.6 while DOE setup is shown in Table 3.7.

Factor	Туре	Levels
Workpiece Type	Categorical	2 (Flat, Curved)
Rotational Speed	Numeric	2 (Low: 250 RPM, High: 750 RPM)
Coolant Flow Rate	Numeric	2 (Low: 20 l/min, High: 30 l/min)

Table 3.6: DOE factors and levels.

This setup made sure a structured exploration of the key factors impacting the coolant flow and subsequently enabled the development of an empirical RSM, which would be useful in predicting coolant performance across varying operating conditions.

Rotational Speed (RPM)	Coolant Flow Rate (l/min)
146.447	25
250	20
250	30
500	17.9289
500	25
500	25
500	25
500	25
500	25
500	32.0711
750	20
750	30
853.553	25
146.447	25
250	20
250	30
500	17.9289
500	25
500	25
500	25
500	25
500	25
500	32.0711
	146.447 250 250 500 500 500 500 500 500 500 750 750 7

Curved	750	20
Curved	750	30
Curved	853.553	25

Table 3.7: DOE simulation matrix showing the factor levels for workpiece type, rotational speed, and coolant flow rate.

3.4. Model Validation Approach

The reliability of the developed CFD model is verified by conducting a series of surrogate experiments with three distinct tools under controlled operating conditions. These experiments serve as substitutes for the commercial Harvi Ultra 8X [52], the tool used in the current study, given that the model was developed on the basis of an idealized tool design. The objective here was to monitor whether the developed CFD model can accurately replicate the coolant flow pattern observed in the real-world conditions. This was required to validate the model's reliability for further applications.

All the experiments were performed on the DECKEL MAHO DMC 850 V CNC Vertical Machining Center, presented in Figure 3.8 [57]. The machine tool was equipped with a high-pressure cooling system and precise tool holders, which enabled a thorough analysis of coolant delivery and its impact on machining. The tools used in the experiments are depicted in Figure 3.9.





Figure 3.8 : Experimental Setup: (a) DECKEL MAHO DMC 850 V CNC Vertical Machining Center and (b) The coolant pump system.

The tool 1 was a Seco Tools milling cutter with an indexable insert, commonly utilized for high-precision milling. The geometry of the tool included a cutting diameter of 25 mm and a functional length of 30 mm. It was equipped with two integrated coolant nozzles that directed the coolant directly to the cutting edge [58]. Tool 2 represented a solid carbide twist drill with an HSK-A63 DIN69893-A tool holder. The tool was well suited for high-speed, high-precision drilling. It had a diameter D of 10 mm with a drilling depth of 5×D and featured two coolant nozzles to generate an optimized internal coolant delivery[59]. Gühring VHM radius cutter was used as the tool 3, which was particularly designed for precision radius milling. The cutting diameter of the tool was 11.5 mm, while it had a length of 120 mm. Compared to tool 1 and tool 2, it had four cooling channels for effectively cooling the machining regions [60].



Figure 3.9 : Tools Used in experiment.

The experiments were conducted under carefully controlled operating parameters. For each tool, a consistent flow rate of water was maintained, and the flow dynamics were observed at three rotational speeds of 200 RPM, 500 RPM, and 1000 RPM. No workpiece was included in the experiments, as the focus was solely on the coolant flow pattern at varying tool rotation. Flow rates applied for each tool are calculated in Table 3.8.

Images of the coolant flow were captured for each experiment. This results in 9 unique images generated from 3 tools at 3 rotational speeds. These snapshots served as the visual representation of the experimental results and were compared with the developed CFD model.

Tool	Measured Coolant	Time (s)	Calculated flow rate (l/min)
	Volume (l)		
Tool 1	2.25	5.73	23.56
Tool 2	1.05	5.83	10.81
Tool 3	1.05	5.74	18.82

 $\begin{table} \textbf{Table 3.8:} Calculated flow rates (l/min) for each tool based on measured coolant volume and time. \\ \end{table}$

The simplified geometry of three tools was incorporated in the defined CFD model, with identical coolant flow rates and rotational speeds as in the experiments. The simulations were executed, and the generated coolant flow fields were placed side by side with the experimental images.

Chapter 4

Results and Discussion

4.1. Model Validation with Experiments

A direct comparison was made between the experimental observations and simulations to establish the reliability of the CFD model. Three surrogate cutting tools were tested under identical coolant flow rates and rotational speeds of 200, 500, and 1000 RPM. The experimental measures were taken as the images of coolant jets for each case, while coolant volume fraction renderings served as the representation of the simulation results. The images were placed side by side for experiments and simulations to evaluate the agreement, as represented by Figure 4.1, Figure 4.2, and Figure 4.3.

At lower rotation speeds (200 RPM), the output showed an excellent match, with the simulation perfectly capturing the coolant jet shape and trajectory. At intermediate speeds (500 RPM), a small deviation was observed as the jet appeared slightly wider in experimental images. Nevertheless, the model could accurately replicate the jet direction and spread despite minor physical disturbances such as mist formation in the experiment, which the CFD inherently smooths out. At higher speed (1000 RPM), the differences between experiment and simulation become a little more apparent. It occurred as coolant jets exhibited more visible atomization and deflection due to the strong centrifugal effects but the differences were not significant enough to undermine the model's predictive power. The coolant coverage and flow field remained closely aligned between both approaches.

The assessment demonstrated that the developed CFD model was capable enough to accurately reproduce the main coolant flow features observed in practice. Minor variations at the high spindle speeds are rooted in the complex physical phenomena, such as droplet breakup, mist formation, and small-scale turbulence, which are difficult to identically replicate in a steady-state CFD model. However, the close overall agreement implied confidence in the developed model, ensuring the model could be relied on for subsequent analysis of coolant delivery performance.

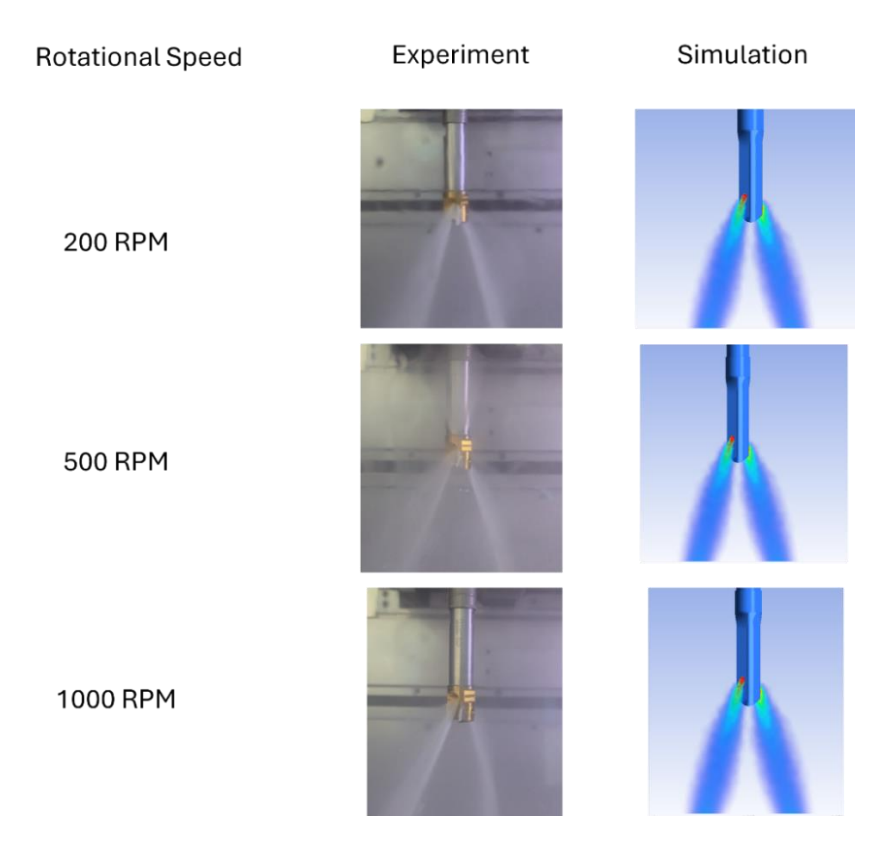


Figure 4.1: Experimental vs. CFD comparison for Tool 1.

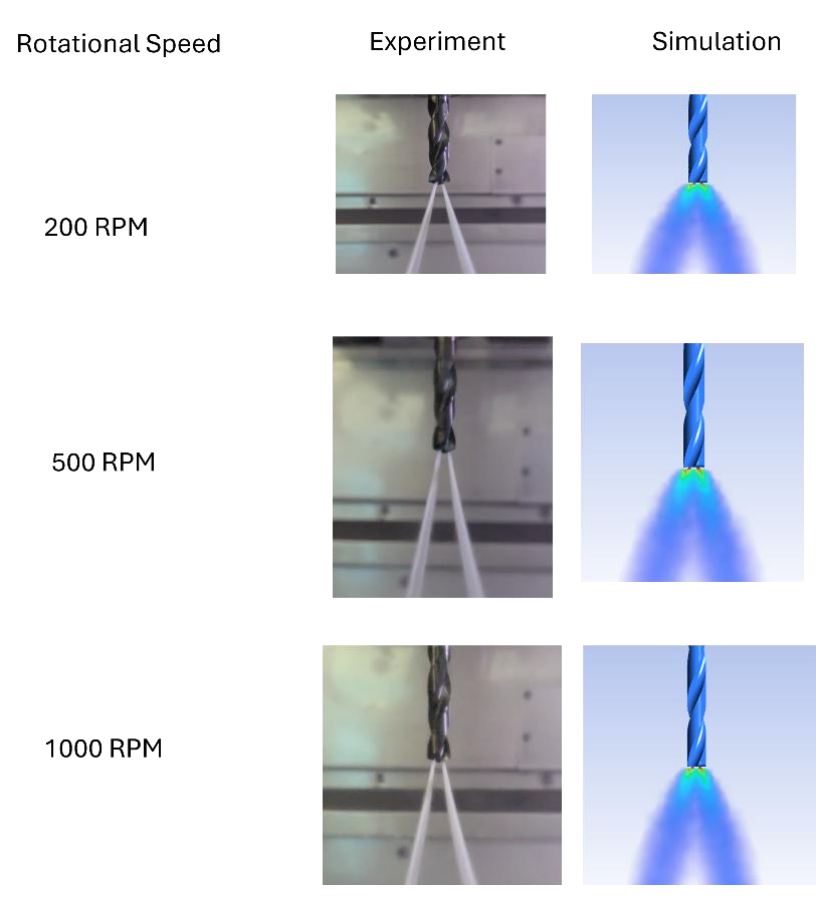


Figure 4.2: Experimental vs. CFD comparison for Tool 2.

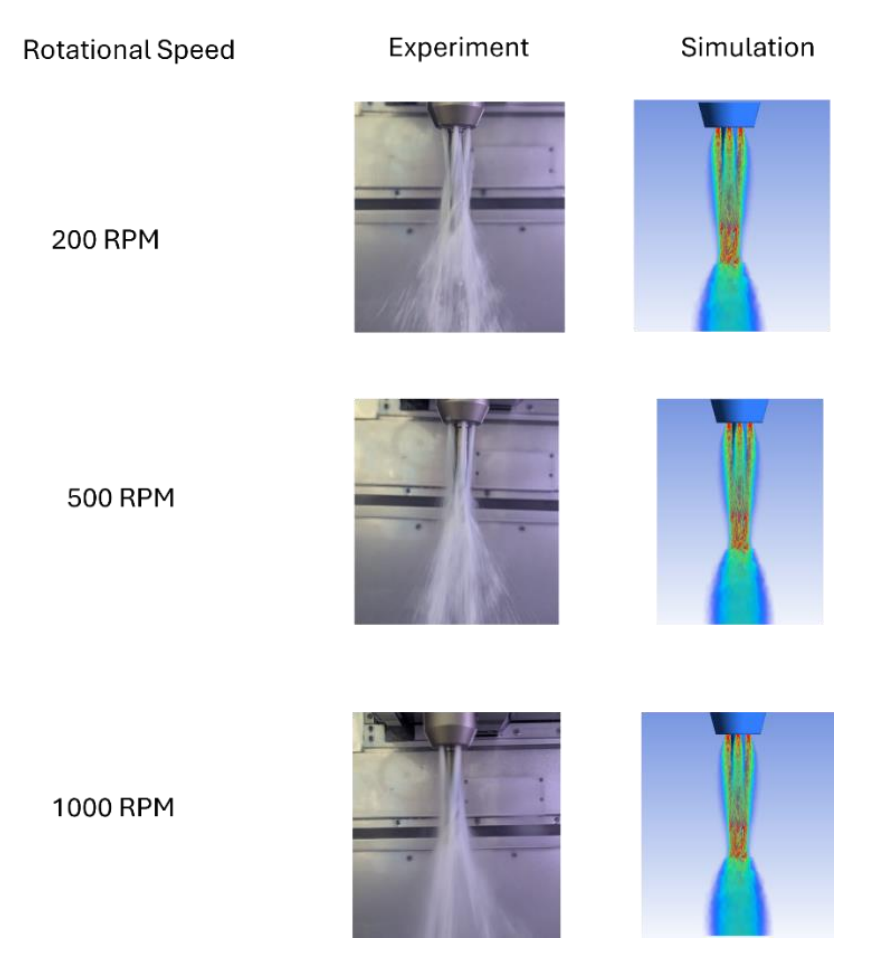


Figure 4.3: Experimental vs. CFD comparison for Tool 3.

4.2. Mesh Independence Test

In computational fluid dynamics (CFD), it is essential that the discretization of the computational domain is done correctly, as the accuracy of the numerical prediction depends on this. While a coarse mesh fails to capture key flow features, a very fine mesh consumes a high computational power without meaningfully improving the accuracy. In addition, there is a possibility that overly fine meshes violate the CFL Condition (Courant–Friedrichs–Lewy condition, $C = a.\frac{\Delta t}{\Delta x} \le 1$, where a is the flow speed, Δt is the time step, and Δx is the cell size). This type of occurrence could hamper the numerical stability unless the time step is adjusted. Therefore, a balance was required to make sure that the optimized computation was utilized while preserving the simulation accuracy. Mesh independence test, a widely adopted technique in the context of CFD, was applied in this study to serve this purpose.

Three mesh densities, coarse, medium, and fine, were generated by modifying the global element size and the local sizing at the nozzle inlet. All other setup parameters, including boundary conditions, solver settings, and physical models, were kept the same. The test was performed under a representative operating condition that utilizes water as a coolant with a flow rate of 25 l/min, in correspondence with a tool rotation of 500 RPM and a workpiece with a flat geometry. The configuration was determined as a baseline to examine the mesh sensitivity with the absence of any additional complexities from variable operating conditions, workpiece geometry, or fluid properties.

Table 4.1 and Table 4.2 represent the number of nodes and elements for each mesh type, along with the key performance parameters monitored in the cutting-zone plane.

For each mesh configuration, the following key coolant flow metrics were recorded at the cutting-zone plane: average coolant velocity (m/s), average coolant volume fraction, coolant coverage area (%), and turbulence kinetic energy (m^2/s^2) .

A significant deviation from medium mesh was observed at the coarse mesh, with velocity reduced by 9.4%, coolant volume fraction increased by 10.3%, coverage area increased by 2.2%, and turbulence kinetic energy reduced by 4.1%. The differences suggested the lack of desired accuracy in resolving coolant flow dynamics at the coarse mesh. In contrast, when the fine mesh was applied, the differences were minimized. For all parameters, deviations remained within the range of 1–2% (velocity -0.58%, volume fraction -1.27%, coverage area -0.95%, and turbulence kinetic energy -0.58%), which is generally considered acceptable in CFD practice.

Mesh	Global Element	Nozzle Inlet	Nodes	Elements
Level	Size (m)	Element Size (m)		
Coarse	0.02	0.005	130,395	630,654
Medium	0.01	0.00050	199,394	930,475
Fine	0.0035	0.00010	281,640	1350,010

Table 4.1: Element sizes and mesh counts for each mesh level.

Mesh	Average Coolant	Average	Coolant	Turbulence
Level	Velocity (m/s)	Coolant	Coverage	Kinetic Energy
		Volume	Area (%)	(m^2/s^2) ,
		Fraction		
Coarse	4.13668	0.141606	69.5478	0.221584
Medium	4.56551	0.128415	68.0248	0.231074
Fine	4.53918	0.126784	67.3815	0.229731

Table 4.2: Key coolant flow metrics for each mesh level.

The differences can be well visualized in Figure 4.4, which depicts the percentage deviation of the coarse and fine meshes compared to the medium mesh across all key parameters. It highlights the close matches of medium mesh with the fine mesh, confirming convergence. Therefore, for all simulations in this study, the medium mesh, with 199,394 nodes and 930,475 elements, was adopted as it confirmed a balance between accuracy and computational efficiency.

Percentage Deviation Between Mesh Types

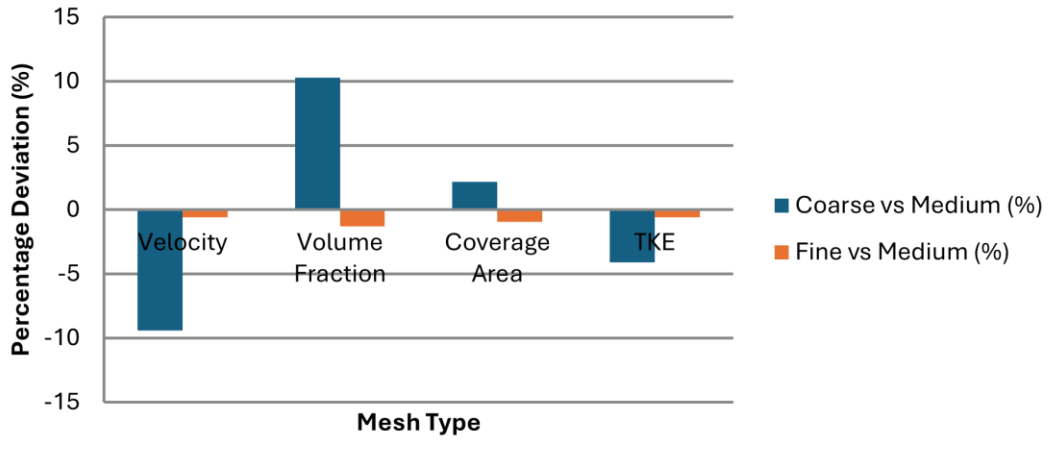


Figure 4.4 : Percentage deviation of coarse and fine mesh results relative to the medium mesh for key flow parameters.

4.3. Influence of Coolant Type

Water and water-based semi-synthetic coolants were employed in the simulation, and their influence on the performance was evaluated in terms of four key parameters: average coolant velocity (m/s), average coolant volume fraction, coolant coverage area (%), and turbulence kinetic energy (m^2/s^2) . To distinctly observe the effect of coolant type, the simulation was executed under a fixed baseline condition of 500 RPM and 25 l/min with the flat-shaped workpiece. The outcome revealed only marginal variations across all parameters and identified their impact on delivery performance to be very similar.

From the ANSYS CFX-Post, it was found that water achieved slightly higher average velocity (4.565 m/s) compared to the semi-synthetic coolant (4.549 m/s). A similar trend was noticed for other parameters also. The coolant volume fraction and coverage area remained slightly higher for water (0.1284 and 68.02% respectively) than the semi-synthetic fluid (0.1279 and 67.71%, respectively). Turbulence kinetic energy values followed the same pattern with water (0.231 m^2/s^2) exceeding the semi-synthetic coolant (0.226 m^2/s^2) by a small margin. Overall, these differences were very minimal within the range of 1% to 2% indicating that coolant type has negligible to no influence on the coolant delivery characteristics under the studied conditions. The key reason for this was due to the very similar viscosity properties of the coolants.

The outcomes are summarized in Figure 4.5, while a comparison of coolant streamlines and volume fraction renderings are depicted in Figure 4.6 and Figure 4.7.

Given that the utilization of the Design of Experiments (DOE) framework in this study was intended to systematically assess the factors that produce significant variation, it was understood that the inclusion of coolant type as a DOE factor would be unnecessary. As the performance differences between water and semi-synthetic coolant are very insignificant, including it would result in substantially increased computational effort without yielding any additional insights.

The finding aligns with the literature that reports that the physical properties of water-based semi-synthetic coolants closely approximate those of pure water, particularly in terms of density and thermal transport behavior. Consequently, comparable hydrodynamic performance in the internal cooling channel was noticed for both fluids. Hence, it was concluded that while coolant type can have a role in tribological aspects of

machining performance, from a purely fluid-flow perspective, the influence is negligible, and it was reasonable to exclude it from the DOE framework.

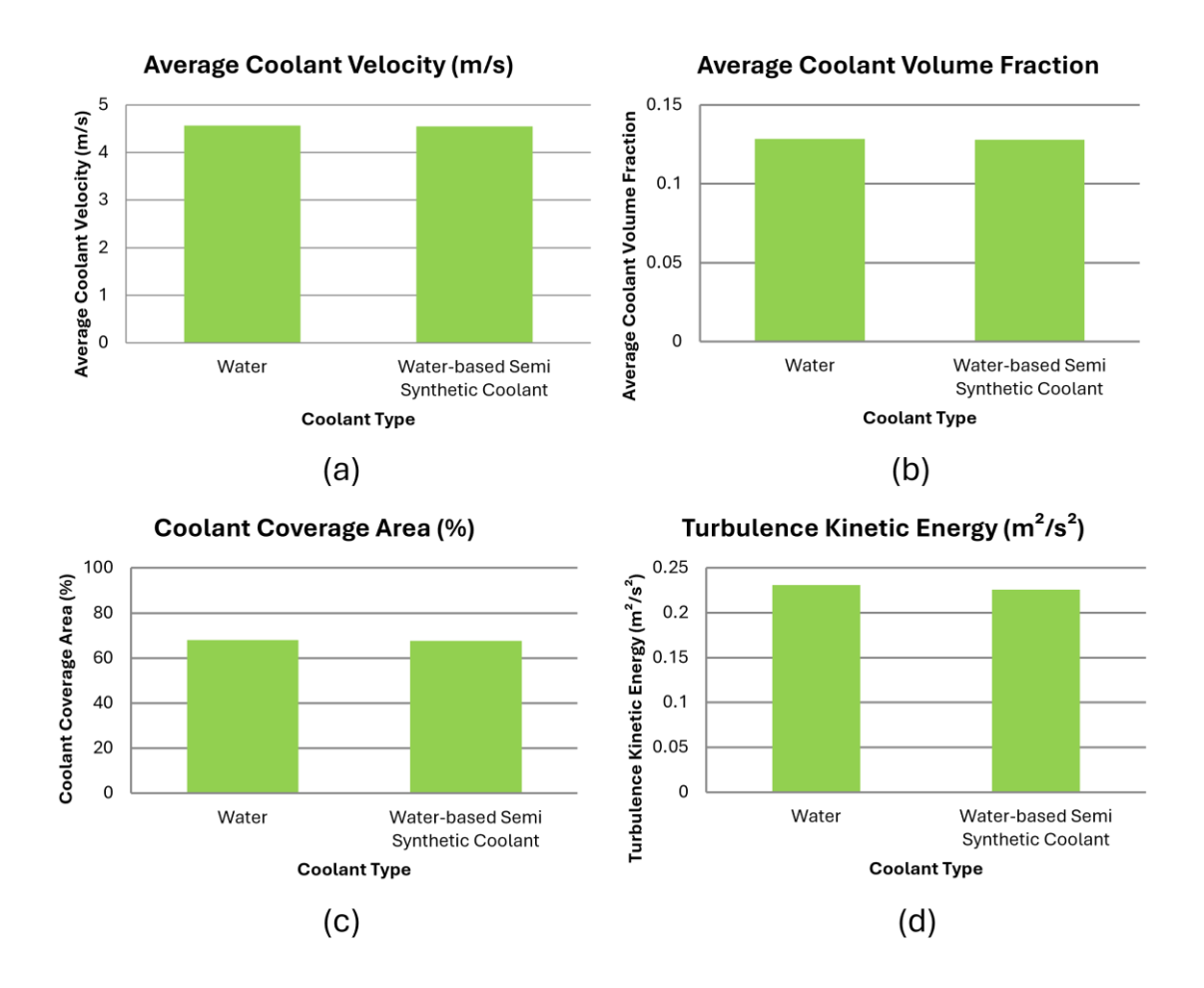


Figure 4.5: Comparison of water and semi-synthetic coolant for (a) Average velocity (m/s), (b) Volume fraction, (c) Coverage area (%), and (d) Turbulence kinetic energy (m^2/s^2) .

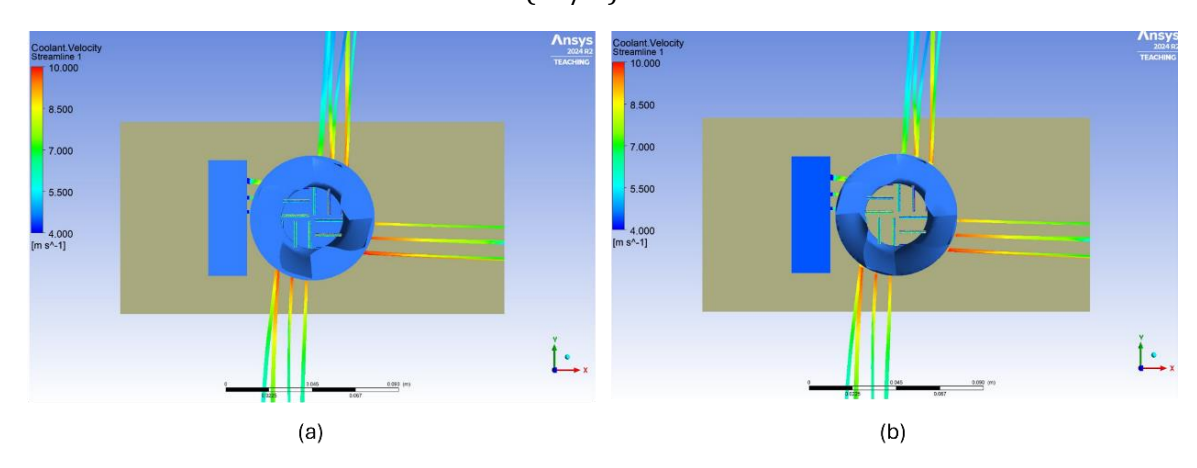


Figure 4.6: Comparison of coolant streamlines for (a) water and (b) semi-synthetic coolant under identical conditions, indicating negligible impact of coolant type on flow behavior.

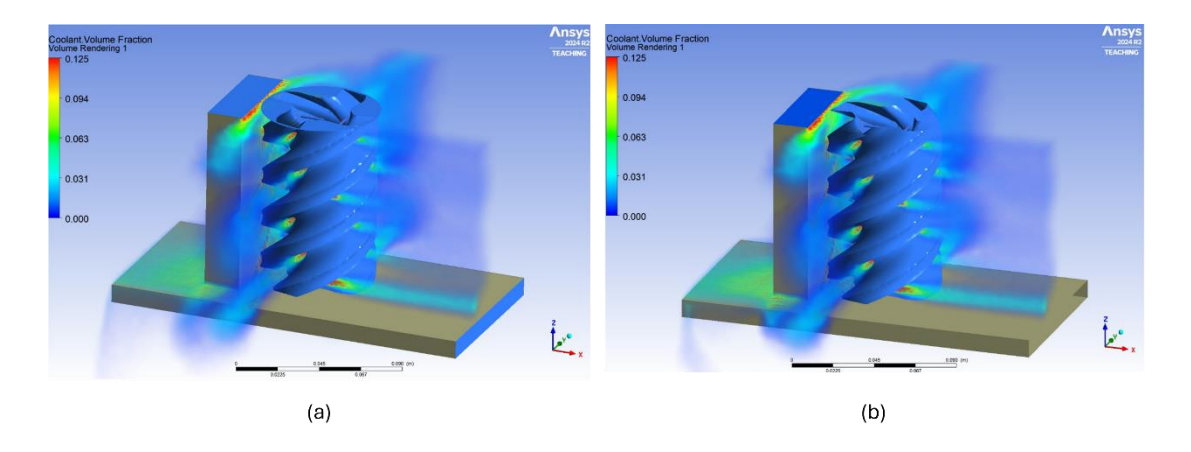


Figure 4.7: Comparison of coolant volume fraction renderings for (a) water and (b) semi-synthetic coolant under identical conditions, indicating negligible impact of coolant type on flow behavior.

4.4. Influence of Operating Parameters and Geometry (DOE Analysis)

As outlined in Chapter 3, the impacts of changing functional conditions and workpiece surface were systematically examined through a Design of Experiment (DOE) framework. Implemented Central Composite Design (CCD) in Minitab enabled the assessment of both linear and quadratic effects for three factors, namely workpiece geometry (flat vs. curved), rotational speed (250–750 RPM), and coolant flow rate (20–30 l/min). In order to construct a robust statistical coverage, a total of 26 simulations were executed.

Four quantifiable response metrics, average coolant velocity, average coolant volume fraction, coolant coverage area, and turbulence kinetic energy (TKE), were extracted from the cutting-zone plate and were employed in the statistical structure. The DOE results were presented and interpreted using Minitab outputs, including summarized ANOVA (Analysis of Variance) table, Pareto chart, main effect plots, response surface plots, and contour plots.

4.4.1. Analysis of Average Coolant Velocity

Table 4.3 depicts the ANOVA P-value summary for average coolant velocity. The values stated that all three primary factors, rotational speed (P = 0.000), coolant flow rate (P = 0.000), and workpiece geometry (P = 0.000), could induce a significant impact at the 95%

confidence level. In terms of two-way interactions, rotational speed \times geometry (P = 0.000) and flow rate \times geometry (P = 0.001) had a considerable effect, while the combined effect of speed \times flow interaction (P = 0.336) did not change the average coolant velocity that much. These findings were further illustrated in the Pareto chart (Figure 4.8). The chart indicates the clear dominance of coolant flow rate (Factor B) in determining the jet's momentum.

	Source	P-Value
	Rotational Speed (RPM)	0.000
Linear	Coolant Flow Rate (l/min)	0.000
Model	Workpiece Type	0.000
Square	Rotational Speed (RPM)×Rotational Speed (RPM)	0.148
Model	Coolant Flow Rate (l/min) ×Coolant Flow Rate (l/min)	0.777
	Rotational Speed (RPM) ×Workpiece Type	0.000
2-Way Interaction	Coolant Flow Rate (l/min) ×Workpiece Type	0.001
Model	Rotational Speed (RPM) ×Coolant Flow Rate (I/min)	0.336

Table 4.3 : ANOVA P-value summary for average coolant velocity.

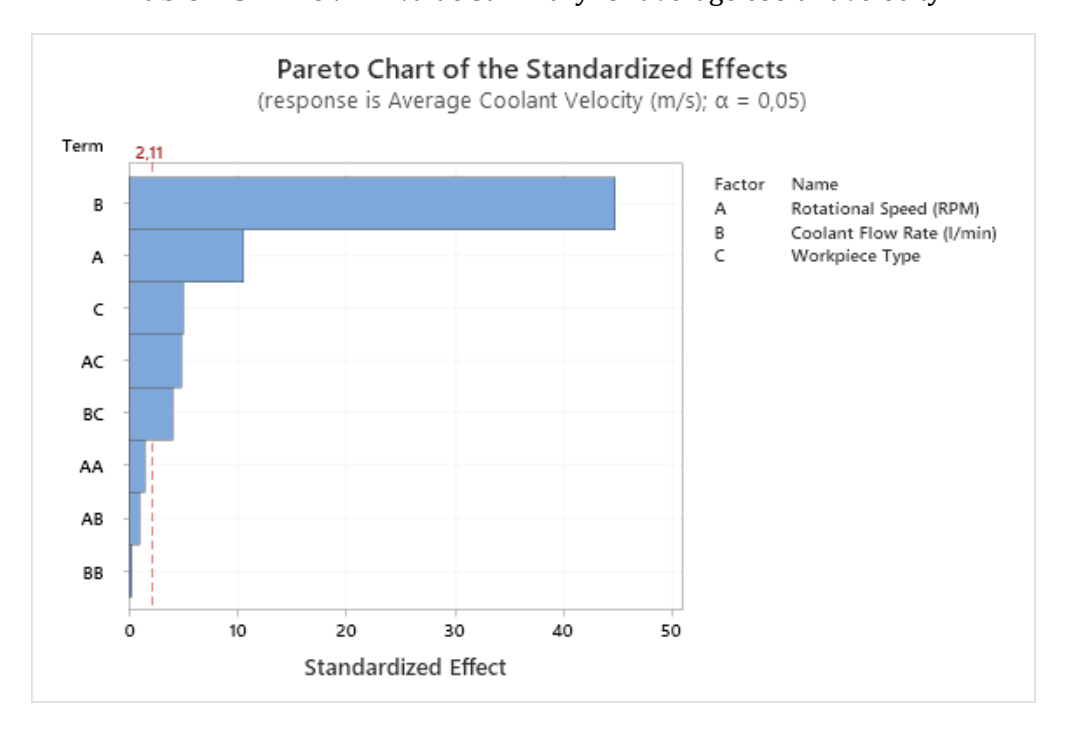


Figure 4.8: Pareto chart of standardized effects for average coolant velocity.

The main effect plots for average coolant velocity are shown in Figure 4.9. As can be seen, the change of coolant flow rate resulted in the steepest slope, confirming the strongest impact on the velocity. Increasing rotational speed also had a positive impact on the velocity, though less pronounced. Shifting from the flat workpiece to the curved workpiece resulted in a slightly higher velocity, but the impact was much less than the coolant flow rate and rotational speed. These findings were consistent with the ANOVA and Pareto results and further confirm the dominance of flow rate in controlling coolant velocity.

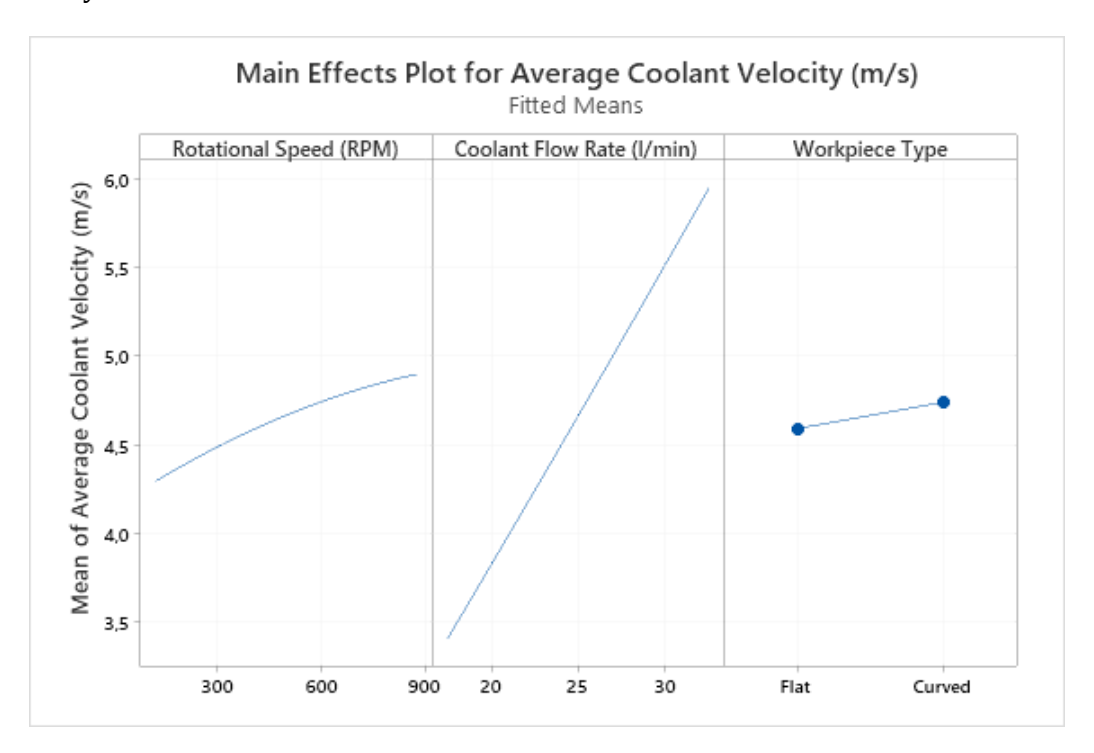


Figure 4.9: Main effect plots for average coolant velocity.

To further investigate the effects of rotational speed and coolant flow rate together, both surface (Figure 4.10) and contour (Figure 4.11) plots were generated for flat and curved workpieces. The plots indicated that coolant velocity increased with both rotational speed and coolant flow rate, while the effect was more visible for the flat workpiece. At high rotational speeds above 750 RPM and flow rates above 30 l/min, coolant velocities exceeded 4.5 m/s and started approaching 6 m/s for both workpiece types. The strongest effect of the coolant factor was also clearly visualized through these plots.

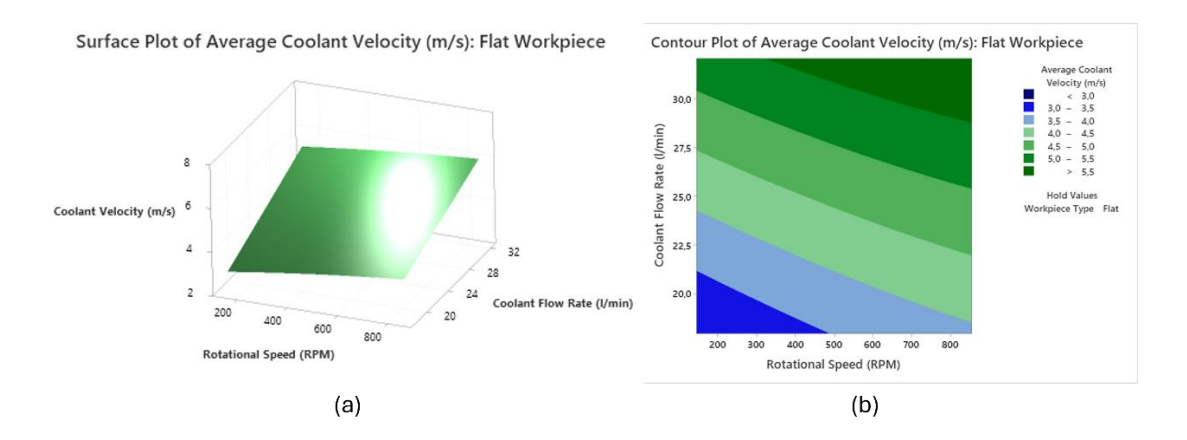


Figure 4.10 : (a) Surface plot of average coolant velocity (m/s) for flat workpiece. (b) Contour plot of average coolant velocity (m/s) for flat workpiece.

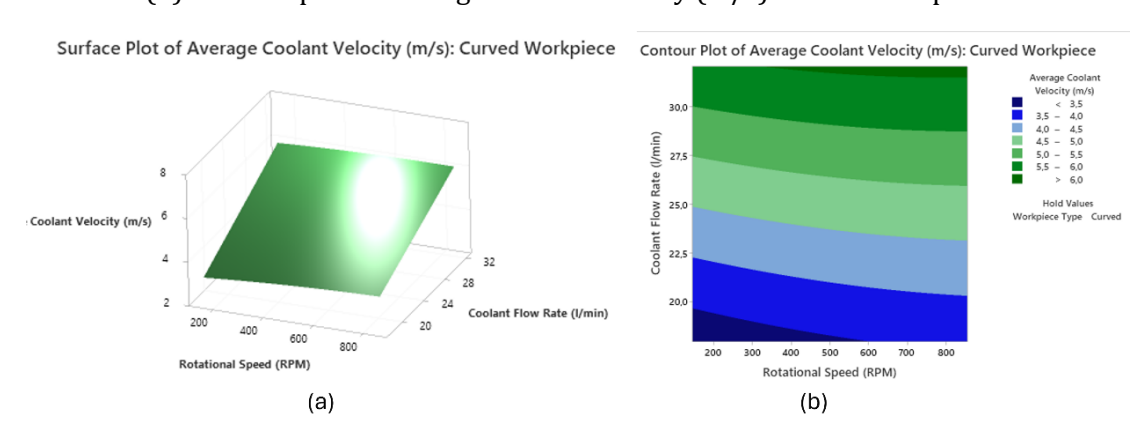


Figure 4.11: (a) Surface plot of average coolant velocity (m/s) for curved workpiece. (b) Contour plot of average coolant velocity (m/s) for curved workpiece.

4.4.2. Analysis of Coolant Volume Fraction

From the ANOVA P-value summary table (Table 4.4) for average coolant volume fraction, it is evident that three primary factors, rotational speed (P = 0.000), coolant flow rate (P = 0.002), and workpiece geometry (P = 0.000), were statistically significant at the 95% confidence level. It was also important to note that the quadratic term for coolant flow rate² (P = 0.016) has some impact, suggesting a non-linear behavior.

Regarding the two-way interactions, the involvement of geometry could induce a considerable impact with speed \times geometry (P = 0.000) and flow \times geometry (P = 0.001). It indicates that the variation in rotational speed or flow rate would have a significant effect, depending heavily on the choice of workpieces. The Pareto chart in Figure 4.12 reinforced this insight, showing the workpiece geometry (Factor C) as the most dominant factor.

	Source	P-Value
	Rotational Speed (RPM)	0.000
Linear	Coolant Flow Rate (l/min)	0.002
Model	Workpiece Type	0.000
Canana	Rotational Speed (RPM)×Rotational Speed (RPM)	0.757
Square Model	Coolant Flow Rate (l/min) ×Coolant Flow Rate (l/min)	0.016
	Rotational Speed (RPM) ×Workpiece Type	0.000
2-Way	Coolant Flow Rate (l/min) ×Workpiece Type	0.001
Interaction Model	Rotational Speed (RPM) ×Coolant Flow Rate (l/min)	0.200

Table 4.4: ANOVA P-value summary for average coolant volume fraction.

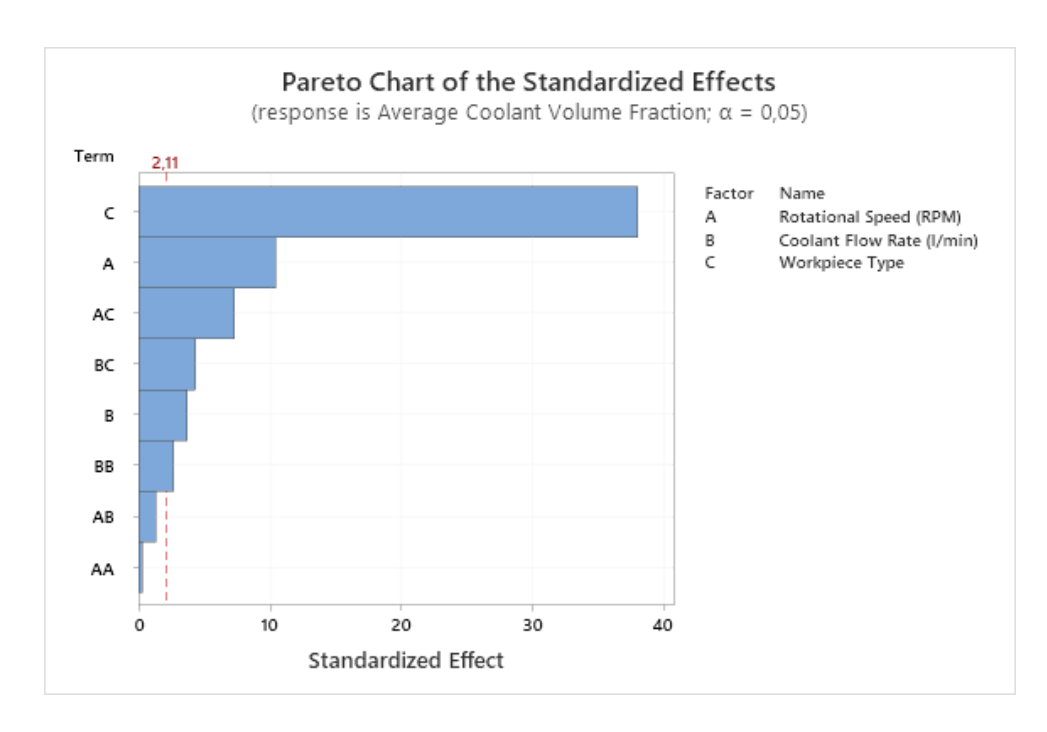


Figure 4.12 : Pareto chart of standardized effects for average coolant volume fraction.

Figure 4.13 presents the main effect plot for average coolant volume fraction. In line with the findings from the ANOVA and Pareto results, workpiece geometry had the strongest influence on coolant concentration, observed by the steepest slope. Compared to the flat surface, curved geometries were able to maintain more coolant at the cutting zone, and it was noted by the consistently higher volume concentrations than flat workpieces. A

moderate decline in coolant volume could be seen with the increase of RPM, as with higher centrifugal forces, coolant could be pushed away further from the cutting zone. The non-linear trend of coolant flow rate from the ANOVA analysis could also be clearly seen on the graph. As the flow rate increased above 25 l/min, the volume fraction reached its peak and started to decrease slowly for high flow rates.

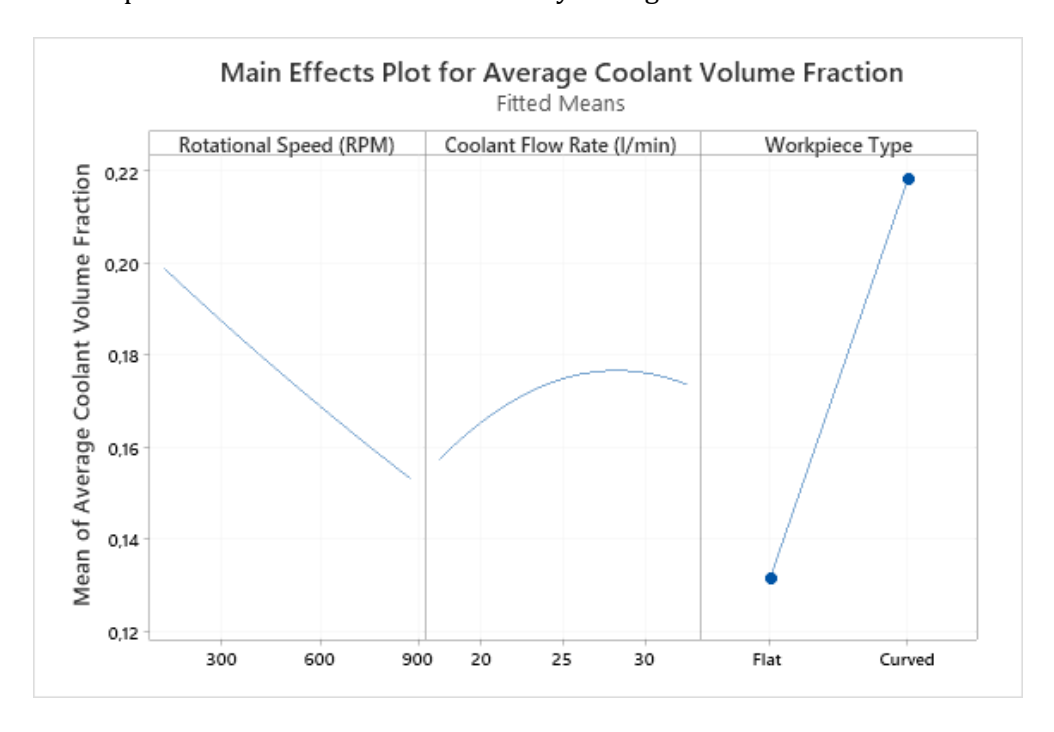


Figure 4.13: Main effect plot for average coolant volume fraction.

Further insights on the combined effects of rotational speed and coolant flow rate on coolant volume fraction were obtained by the response (Figure 4.14) and contour plots (Figure 4.15) for both sets of workpieces. The curved geometry generated a much higher value of volume fractions (exceeding 0.22), in comparison to the flat workpiece (surpassing 0.16) at the similar operating range.

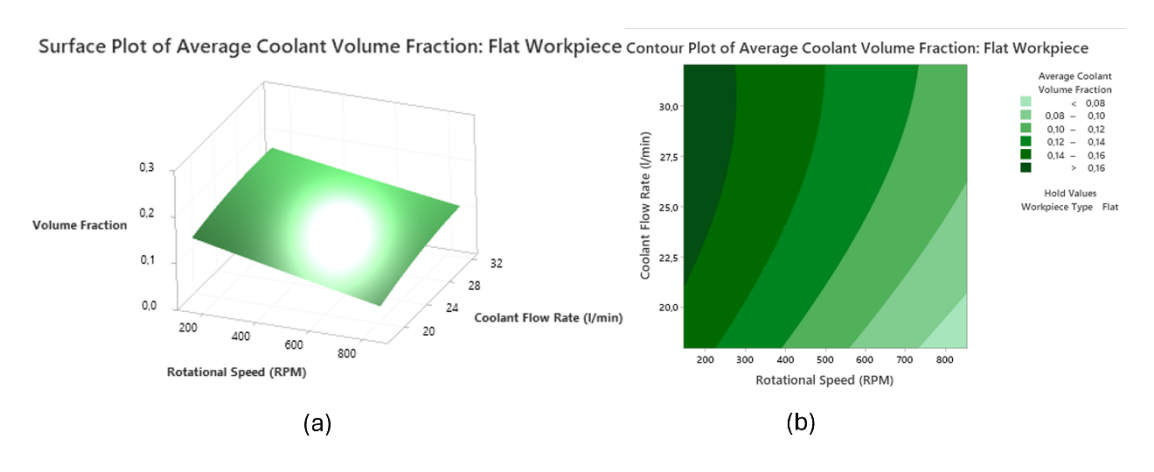


Figure 4.14 : (a) Surface plot of average coolant volume fraction for flat workpiece. (b) Contour plot of average coolant volume fraction for flat workpiece.

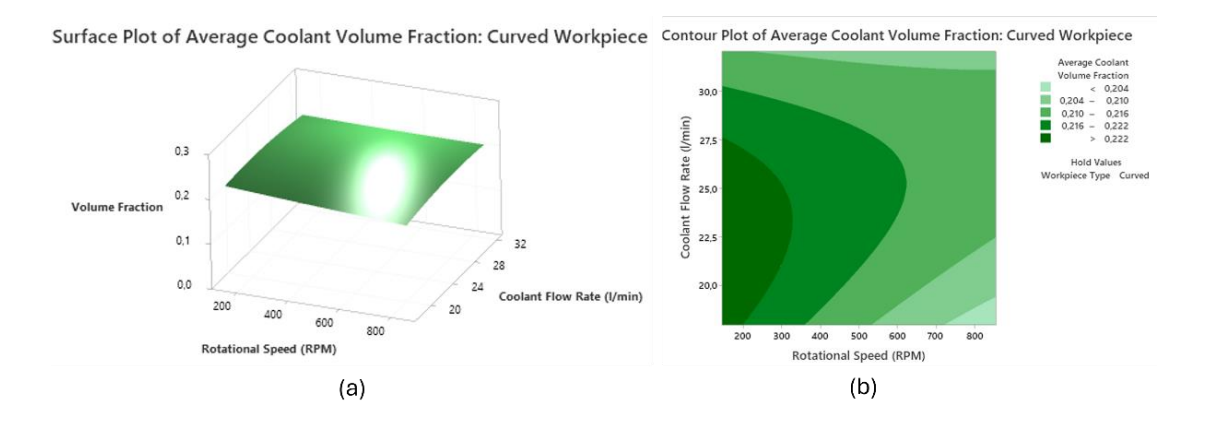


Figure 4.15 : (a) Surface plot of average coolant volume fraction for curved workpiece. (b) Contour plot of average coolant volume fraction for curved workpiece.

4.4.3. Analysis of Coolant Coverage Area (%)

Outcomes from ANOVA P-value summary (Table 4.5) found that all three main factors, rotational speed (P = 0.000), coolant flow rate (P = 0.001), and workpiece geometry (P = 0.000), were statistically important at the 95% confidence level.

Similar behavior to coolant volume fraction regarding two-way interactions was observed for coolant coverage area (%). Like the coolant volume fraction, the involvement of geometry with rotational speed (P = 0.000) or coolant flow rate (P = 0.000) resulted in a considerable impact. This implies that the shape of the workpiece strongly influenced how widely the coolant is distributed across the cutting zone. The Pareto chart in Figure 4.16 represents workpiece geometry (C) as the most influential factor, followed by the interaction of rotational speed and workpiece geometry (C) and rotational speed alone (C).

The main effect plots in Figure 4.17 also depict the significance of workpiece geometry with a steep slope. Curved workpieces showed a significantly higher coverage area, as the surface curvature enhanced the coolant distribution across the cutting zone. Rotational speed also had a noticeable effect, indicated by a sharp negative slope. As the RPM increased from 250 to 750 RPM, the centrifugal force deflected the coolant away from the targeted region, thereby reducing effective coverage.

	Source	P-Value
	Rotational Speed (RPM)	0.000
Linear	Coolant Flow Rate (l/min)	0.001
Model	Workpiece Type	0.000
_	Rotational Speed (RPM)×Rotational Speed (RPM)	0.585
Square Model	Coolant Flow Rate (l/min) ×Coolant Flow Rate (l/min)	0.620
	Rotational Speed (RPM) ×Workpiece Type	0.000
2-Way Interaction Model	Coolant Flow Rate (l/min) ×Workpiece Type	0.000
	Rotational Speed (RPM) ×Coolant Flow Rate (l/min)	0.206

Table 4.5: ANOVA P-value summary for coolant coverage area (%).

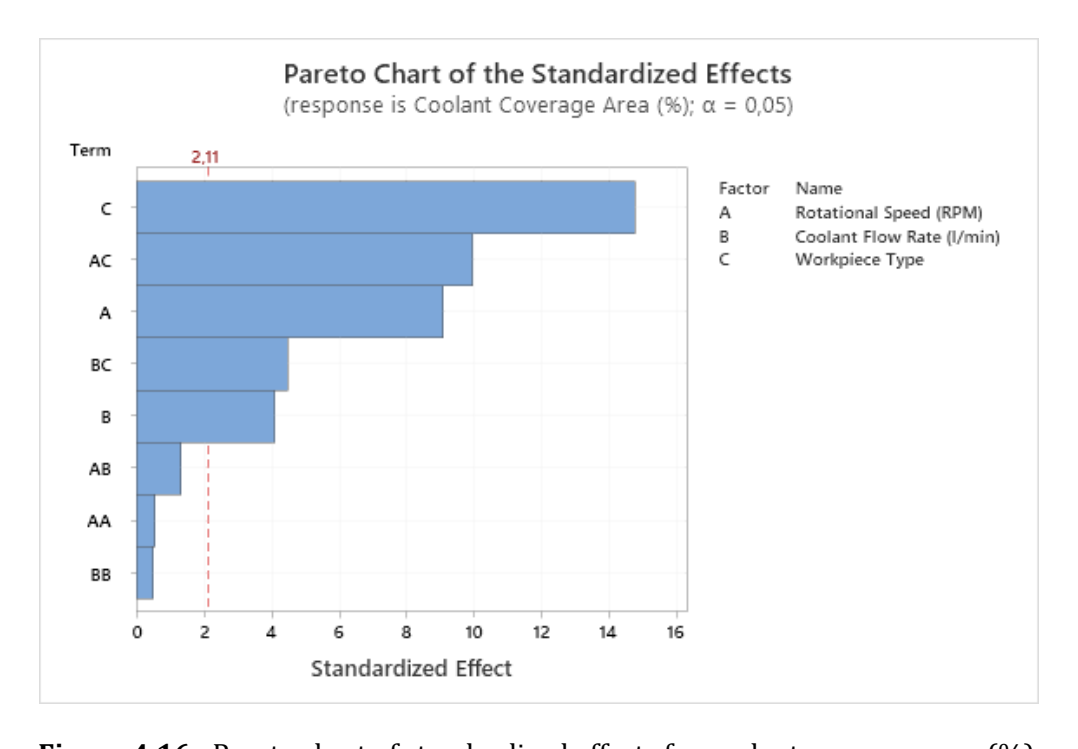


Figure 4.16: Pareto chart of standardized effects for coolant coverage area (%).

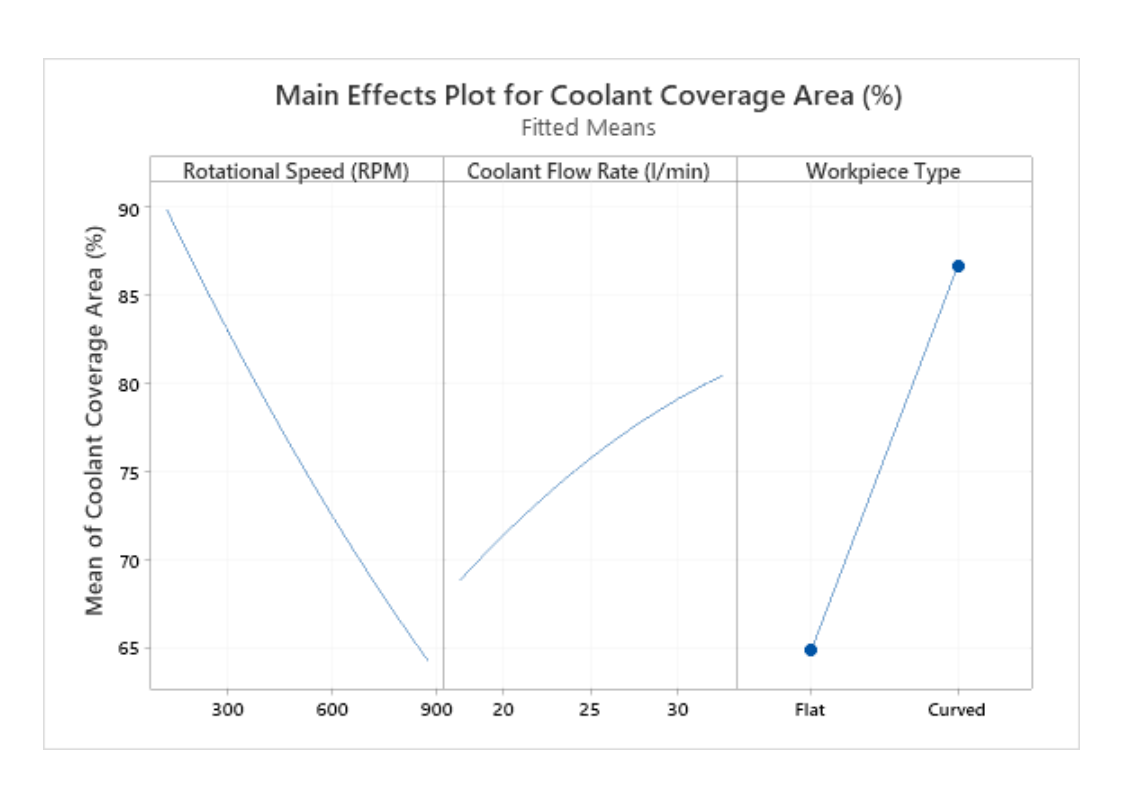


Figure 4.17: Main effect plots for coolant coverage area (%).

Surface plots and contour plots for both flat and curved workpieces are shown in Figure 4.18 and Figure 4.19. The curved geometry clearly achieved high coverage across the whole operating range, never under 80%. On the other hand, results showed a high dependency of performance on the rotational speed for flat geometry. With the increase of RPM above 500, the coolant coverage area fell rapidly, even below 40% with very high tool rotation and low coolant flow rate. The contour plot for curved workpiece represents an interesting outlook on the combined effect of rotational speed and coolant flow rate, depicted by Figure 4.19.

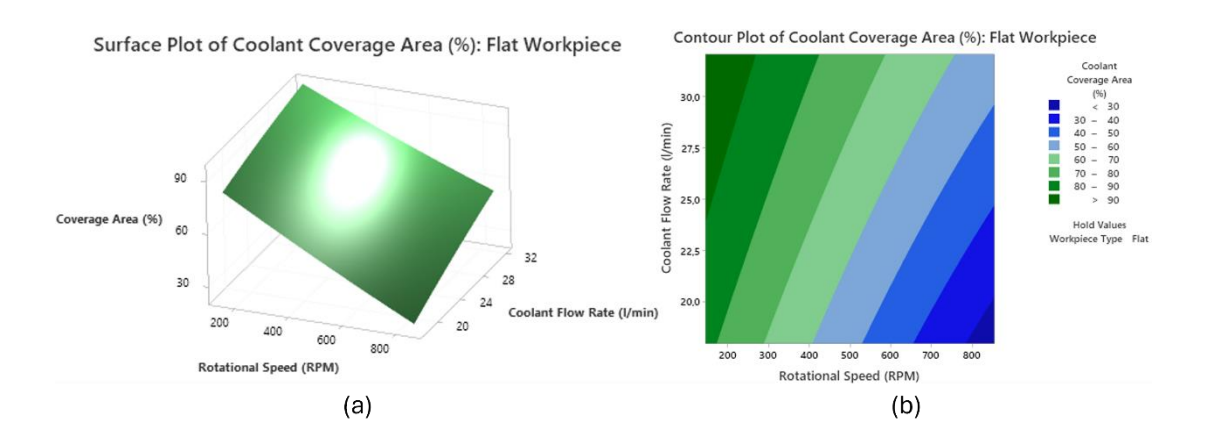


Figure 4.18 : (a) Surface plot of coolant coverage area (%) for flat workpiece. (b) Contour plot of coolant coverage area (%) for flat workpiece.

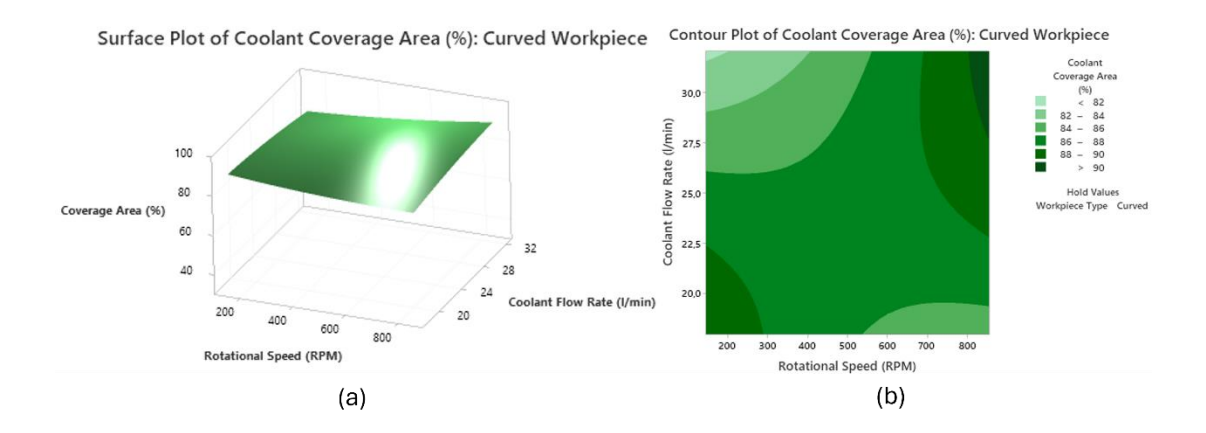


Figure 4.19: (a) Surface plot of coolant coverage area (%) for curved workpiece. (b) Contour plot of coolant coverage area (%) for curved workpiece.

4.4.4. Analysis of Turbulence Kinetic Energy

(TKE)

Table 4.6 presents ANOVA P-value summary, demonstrating the strong relevance of all three primary factors, rotational speed (P = 0.001), coolant flow rate (P = 0.000), and workpiece geometry (P = 0.000). at the 95% confidence level. In addition, the quadratic term of coolant flow rate² (P = 0.009) was found to be notable, suggesting non-linear behavior. Regarding two-way interactions, rotational speed × geometry (P = 0.000) and flow rate × geometry (P = 0.000) were significant, indicating the differences in effects on flat and curved workpieces. The Pareto chart from Figure 4.20 highlights the stark dominance of coolant flow rate (P = 0.000) over other factors, implying the vital role of flow rate in modulating turbulence levels.

Figure 4.21 presents the main effect plots for turbulence kinetic energy (TKE). Coolant flow rate showed the most pronounced effect, as the turbulence intensity increased sharply with the higher coolant flow. A slight non-linearity in the increase aligned well with the analysis from the ANOVA results. Workpiece geometry showed a measurable influence, but not as strong as the coolant flow rate. The curved workpiece, due to its surface curvature, promoted enhanced coolant mixing and jet instability, resulting in higher TKE. The rotational speed also had a weak but noticeable influence, as the TKE increased gradually with the increase in RPM.

	Source	P-Value
	Rotational Speed (RPM)	0.001
Linear Model	Coolant Flow Rate (l/min)	0.000
	Workpiece Type	0.000
C	Rotational Speed (RPM)×Rotational Speed (RPM)	0.485
Square Model	Coolant Flow Rate (l/min) ×Coolant Flow Rate (l/min)	0.009
	Rotational Speed (RPM) ×Workpiece Type	0.000
2-Way Interaction Model	Coolant Flow Rate (l/min) ×Workpiece Type	0.000
	Rotational Speed (RPM) ×Coolant Flow Rate (I/min)	0.391

Table 4.6: ANOVA P-value summary for turbulence kinetic energy (TKE).

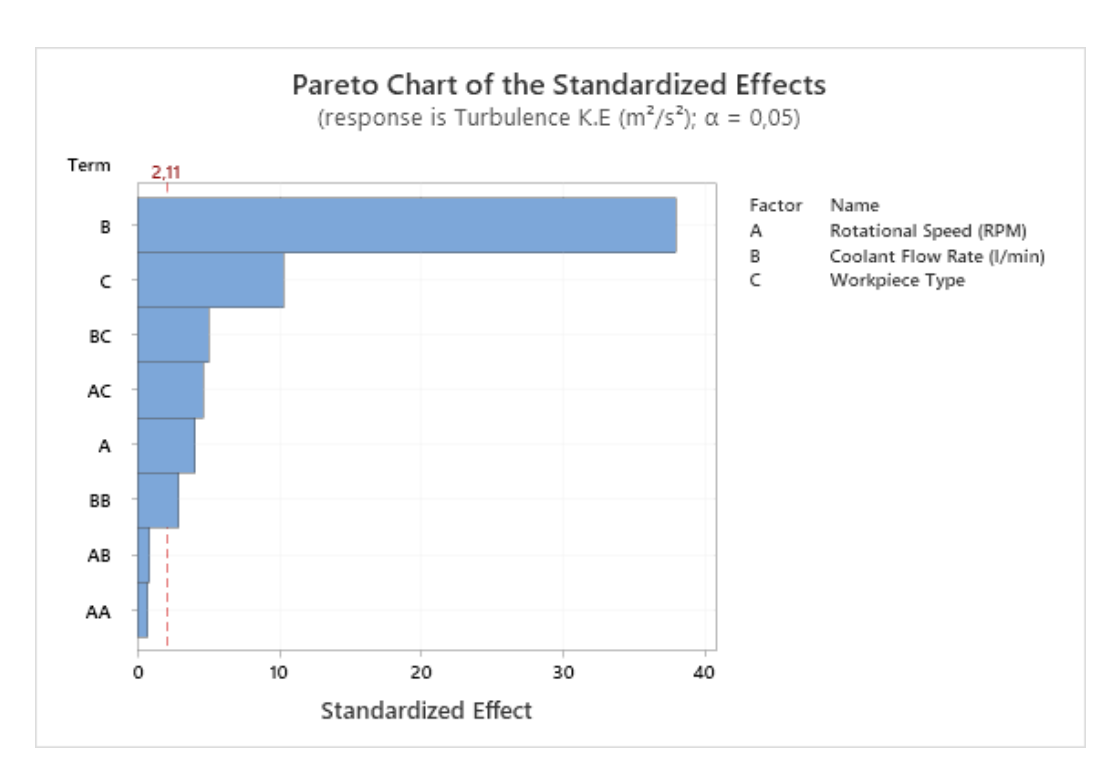


Figure 4.20: Pareto chart of standardized effects for turbulence kinetic energy (TKE).

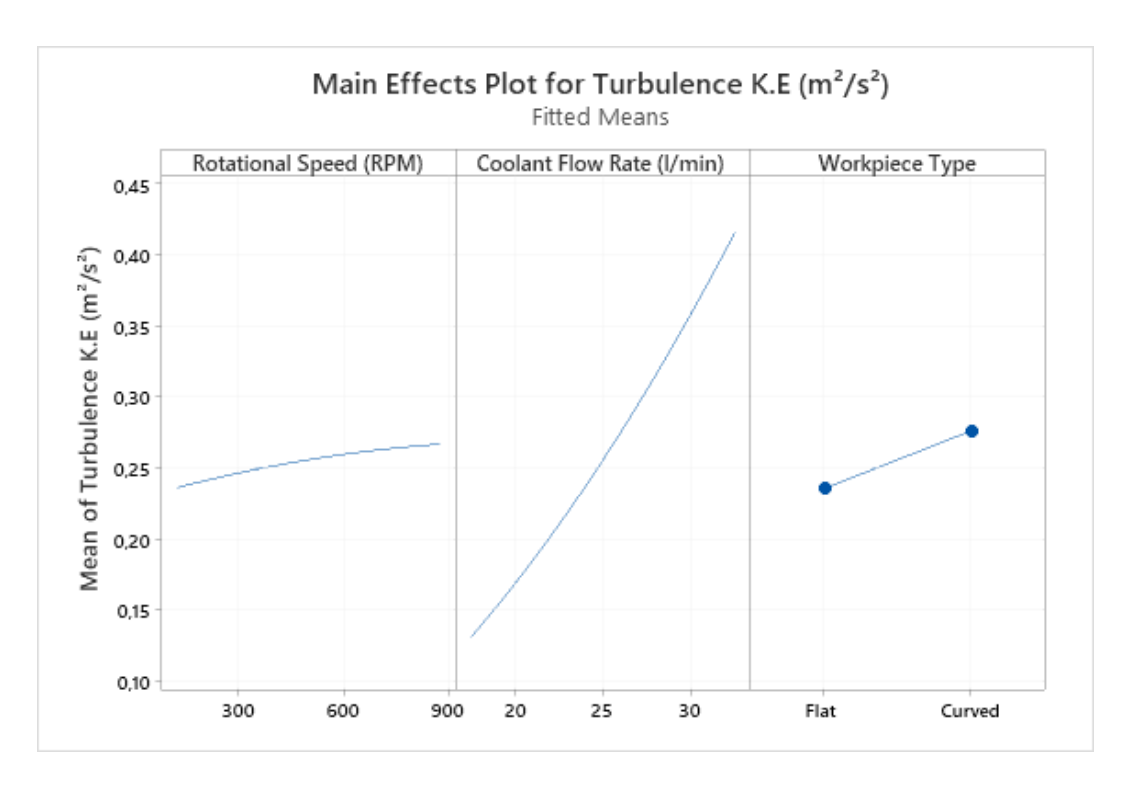


Figure 4.21: Main effect plots for turbulence kinetic energy (TKE).

The surface (Figure 4.22) and contour (Figure 4.23) plots for turbulence kinetic energy (TKE) under both flat and curved workpieces depicted that TKE increased with both rotational speed and coolant flow rate. However, the much stronger impact of coolant flow rate was clearly visualized for both cases. The contour plots revealed that the turbulence remained below $0.20~\text{m}^2/\text{s}^2$ at lower flow rates around 20~l/min, even at medium to high spindle speeds of around 500 RPM, while exceeding $0.35~\text{m}^2/\text{s}^2$ at high flow rates of 30~l/min and low RPM of around 250.

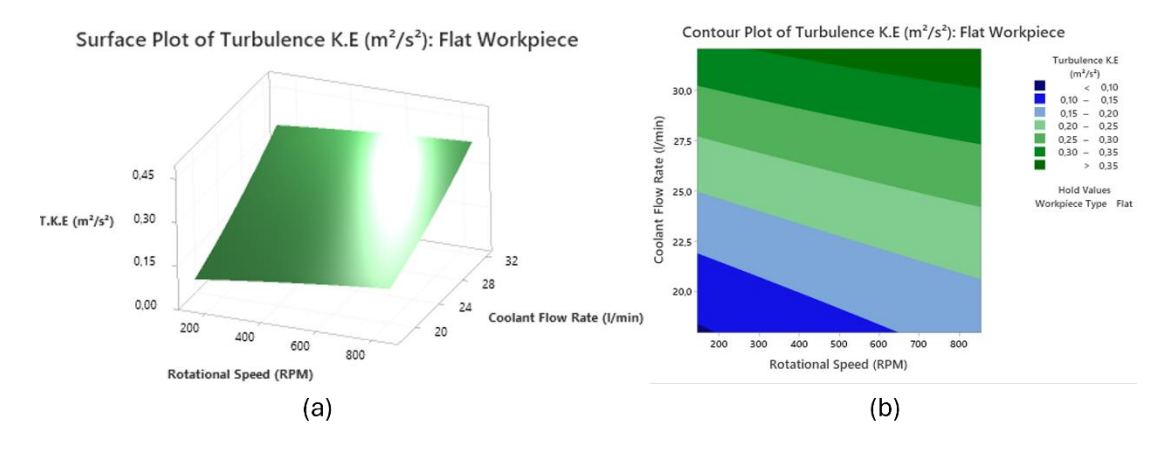


Figure 4.22 : (a) Surface plot of turbulence kinetic energy (m²/s²) for flat workpiece. (b) Contour plot of turbulence kinetic energy (m²/s²) for flat workpiece.

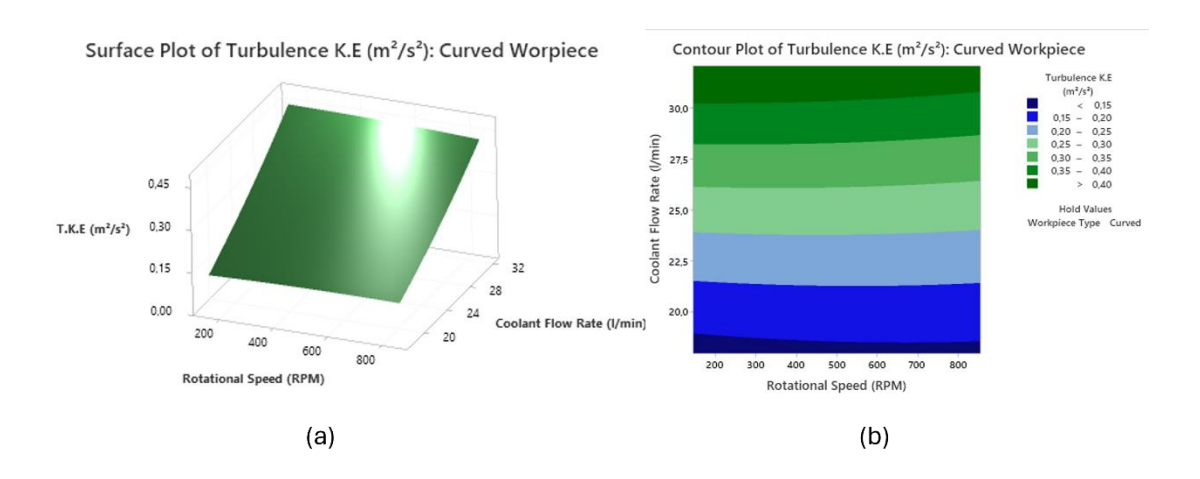


Figure 4.23 : (a) Surface plot of turbulence kinetic Energy (m²/s²) for curved workpiece. (b) Contour plot of turbulence kinetic energy (m²/s²) for curved workpiece.

4.4.5. Summary of DOE Results

The structure of Design of Experiments (DOE) allowed a comprehensive understanding of each factor, workpiece geometry, rotational speed and coolant flow rate's influence on coolant delivery performance. The responses were evaluated separately in terms of average coolant velocity, coolant volume fraction, coolant coverage area, and turbulence kinetic energy (TKE) and an in depth insight was achieved. Complete tabulated results for all DOE operating conditions are attached in Appendix A.

Table 4.7 confirm that the coolant flow rate was the most responsible for altering the average coolant velocity and turbulence kinetic energy, as the increase in flow strongly enhanced the jet momentum and turbulence intensity. The influences were sometimes nonlinear, showing diminishing returns at higher levels. On the other hand, variation of workpiece geometry exerted the greatest influence on volume fraction and coverage area. The shift from flat to curved surface generated better performance across all operating parameters. Rotational Speed played a secondary but contrasting role in impacting average coolant velocity, turbulence kinetic energy and coolant volume fraction, coolant coverage area. It increased velocity and turbulence but showed a negative effect on volume fraction and coverage, where higher RPM deflected coolant away from the cutting zone. Interaction effects involving geometry were significant in all cases, indicating that operating parameters behave differently depending on the workpiece surface shape.

Response Metric	Dominant Factor	Secondary Factors	Notable
			Interactions
Average Coolant	Flow rate (+)	Speed (+), Geometry	Flow × Geometry,
Velocity		(Curved > Flat)	Speed ×
			Geometry
Coolant Volume	Geometry (Curved	Speed (-), Flow (+)	Flow × Geometry,
Fraction	> Flat)		Speed ×
			Geometry
Coolant Coverage	Geometry (Curved	Flow (+)	Flow × Geometry,
Area (%)	> Flat), Speed (-)		Speed ×
			Geometry
Turbulence Kinetic	Flow rate (+,	Geometry (+), Speed	Flow × Geometry,
Energy (TKE)	nonlinear)	(+)	Speed ×
			Geometry

Table 4.7 : Summary of factor significance across response metrics (+ = positive effect, - = negative effect).

From the DOE analysis, it can be summarized that flow rate governs jet momentum and turbulence, geometry controls retention and coverage, and spindle speed modifies these effects, either reinforcing them, such as for velocity, TKE, or reducing them, as for volume fraction and coverage.

Appendix B contains the regression equations developed for the four output responses (average coolant velocity, coolant volume fraction, coolant coverage area, and turbulence kinetic energy).

Chapter 5

Conclusion and Future Work

The study was aimed at investigating the stand alone and combined influence of workpiece geometry, tool rotation, and coolant flow rate on coolant delivery performance in internally cooled milling operations. For the analysis, a CFD model was created and backed by surrogated experimental validation. The simulations were carried out following a structured Design of Experiments (DOE) framework and the outcomes were reported as four key coolant delivery metrics: average coolant velocity, coolant volume fraction, coolant coverage area, and turbulence kinetic energy (TKE). The findings generated a clear understanding of coolant performance in dynamic machining scenarios and have established the developed CFD model as a reliable predictive tool.

The outcomes of the research can be summarized in following points.

- The change in coolant type did not influence the delivery performance. The comparison between water and water-based semi-synthetic coolant showed only 1-2% differences between each other across all performance indicators.
- Coolant flow rate directly controls jet momentum and turbulence intensity. The
 increase in flow consistently could enhance both velocity and TKE, but the
 intensity diminished at higher levels.
- The choice of workpiece geometry played a decisive role in coolant retention and distribution. In all cases, curved geometries performed far better indicated by higher volume fractions and coverage areas. This confirms the implications of using curved geometries in maintaining stable coolant delivery to the cutting zone.
- Rotational speed was recognized as a secondary but influential factor, particularly at higher levels. The high spindle speeds contributed to increased velocity and turbulence, but at the same time significantly deteriorated coolant fraction and coverage at the target zone.
- All interaction effects, including geometry, had a considerable impact on the performance metrics. It highlighted that any effort to parameter optimization must consider geometry-specific responses.

The study demonstrated novelty in coupling CFD simulations with a structured CFD approach. Particularly for widely adopted internally cooled milling, the analysis brings practical value to systematically analyze the coolant delivery. The insights gathered would be useful in machining hard to cut advanced materials and hence accelerating the industry 4.0 applications. In addition, the validated computational model could work as a cost and time-effective alternative to extensive experimental trials, while also providing detailed insights that are difficult to obtain from physical setups. The output from the study directly relates tool design with machining process planning and has the potential to guide the development of geometry-adaptive cooling systems. Furthermore, the CFD model developed here would serve as a basis for future simulations-based studies involving the cooling performance in machining.

The current study naturally falls under some limitations that could be improved further. The sole focus of the research was to examine the hydrodynamic behavior of the coolant. The simulation was conducted at isothermal, steady-state conditions, and it did not consider heat transfer, droplet atomization, and thermal stresses to minimize the complexity. The phenomenon observed in experimental rigs, such as mist formation and fine-scale turbulence at high spindle speed, was challenging to recreate in the CFD simulations. In addition, the tools used in the model were simplified representations of a commercial cutter, which, while it was able to provide accurate measures on the flow field, did not fully capture the complexities of industrial tool geometries.

These limitations open several promising aspects on which future research could be conducted. First comes the integration of heat transfer and thermal stress into the developed CFD simulations, which would provide a more complete picture of cooling effectiveness and tool-workpiece interactions. Further, it would enhance the results if the model were extended to transient conditions, allowing better analysis of intermittent cutting phenomena. Next, the insights from the work could be implemented in designing optimized cooling channels. Cutting tools with added complexities could be tested, and better comprehensive evaluation could be made on the industrial applicability. Finally, an interesting approach would be to incorporate advanced methods such as machine learning into the simulation workflow. It would enable much faster and more accurate prediction of flow behavior while also supporting real-time optimization.

To conclude, the research was successful at meeting the objectives of the study outlined at the beginning. The developed CFD model has been validated through surrogated experiments and has been enhanced by DOE methods, and proves to be a powerful tool for understanding and optimizing coolant delivery in milling with internal supply systems. The importance of tailoring coolant strategies in response to the operating conditions and workpiece geometry was reaffirmed by the outcomes. The study, most importantly, establishes a robust foundation upon which future developments in sustainable, high-performance machining can be achieved.

Appendix A

Detailed CFD Results for Flat and Curved Workpieces

Extracted results for all simulation results are displayed in this section. Table A.1 and Table A.2 include obtained values of average coolant velocity, coolant volume fraction, coolant coverage area, and turbulence kinetic energy (TKE) for all tested rotational speeds and flow rates for flat and curved workpieces.

RPM	Flow Rate (l/min)	Average Coolant Velocity (m/s)	Average Coolant Volume Fraction	Coolant Coverage Area (%)	Turbulence Kinetic Energy (m²/s²)
146.447	25	4.220	0.170	89.01	0.213
250	20	3.495	0.144	76.16	0.138
250	30	5.030	0.171	86.18	0.302
500	17.9289	3.430	0.111	51.39	0.127
500	25	4.566	0.128	68.02	0.231
500	32.0711	5.721	0.137	71.46	0.366
750	20	4.194	0.089	32.85	0.189
750	30	5.589	0.120	59.27	0.344
853.553	25	4.988	0.100	37.08	0.271

Table A.1: CFD outcomes for flat workpiece under DOE operating conditions.

		Average	Average	Coolant	Turbulence
RPM	Flow Rate	Coolant	Coolant	Coverage	Kinetic
	(l/min)	Velocity	Volume	Area (%)	Energy
		(m/s)	Fraction		(m^2/s^2)
146.447	25	4.448	0.225	88.71	0.264
250	20	3.735	0.215	86.21	0.179
250	30	5.468	0.214	89.86	0.381
500	17.9289	3.357	0.220	90.18	0.132
500	25	4.767	0.221	83.54	0.280
500	32.0711	6.194	0.204	84.57	0.465
750	20	3.987	0.195	88.89	0.181
750	30	5.649	0.213	90.16	0.368
853.553	25	4.752	0.213	91.38	0.263

 $\textbf{Table A.2:} \ \textbf{CFD outcomes for curved workpiece under DOE operating conditions.}$

Appendix B

Regression Equations for Output Responses

From the DOE analysis, following regression equations were obtained for the four output responses, average coolant velocity (m/s), average coolant volume fraction, coolant coverage area (%), and turbulence kinetic energy (m^2/s^2). The equations are expressed in actual operating units (RPM and l/min).

- 1. Average Coolant Velocity (m/s)
 - Flat workpiece:

$$V = -0.092 + 0.002195 \times RPM + 0.1531 \times Q + 0.000234 \times Q^{2}$$

$$- 0.000021 \times (RPM \times Q)$$
(B.1)

• Curved workpiece:

$$V = -0.348 + 0.001456 \times RPM + 0.1841 \times Q + 0.000234 \times Q^{2}$$

$$-0.000021 \times (RPM \times Q)$$
(B.2)

- 2. Average Coolant Volume Fraction
 - Flat workpiece:

$$\phi = 0.0499 - 0.000165 \times \text{RPM} + 0.00958 \times Q - 0.000167 \times Q^2 + 0.000002$$

$$\times (\text{RPM} \times Q)$$
(B.3)

• Curved workpiece:

$$\phi = 0.1568 - 0.000081 \times RPM + 0.00707 \times Q - 0.000167 \times Q^2 + 0.000002$$

$$\times (RPM \times Q)$$
(B.4)

3. Coolant Coverage Area (%)

• Flat workpiece:

A =
$$67.3 - 0.1159 \times \text{RPM} + 1.94 \times \text{Q} - 0.000009 \times \text{RPM}^2 - 0.0204 \times Q^2 + 0.00140 \times (\text{RPM} \times \text{Q})$$
 (B.5)

• Curved workpiece:

$$A = 93.9 - 0.0407 \times RPM + 0.25 \times Q - 0.000009 \times RPM^{2} - 0.0204 \times Q^{2} + 0.00140 \times (RPM \times Q)$$
(B.6)

- 4. Turbulence Kinetic Energy (m²/s²)
 - Flat workpiece:

TKE =
$$-0.0611 + 0.000180 \times \text{RPM} + 0.00196 \times \text{Q} + 0.000314 \times$$

$$Q^2 - 0.000002 \times (\text{RPM} \times \text{Q})$$
(B.7)

• Curved workpiece:

TKE =
$$-0.0999 + 0.000087 \times \text{RPM} + 0.00700 \times \text{Q} + 0.000314 \times Q^2 -$$

$$0.000002 \times (\text{RPM} \times \text{Q})$$
(B.8)

Bibliography

- [1] Wit. Grzesik, Advanced machining processes of metallic materials: theory, modelling and applications. Elsevier, 2008.
- [2] K. Huang and W. Yang, "Analytical model of temperature field in workpiece machined surface layer in orthogonal cutting," *J Mater Process Technol*, vol. 229, pp. 375–389, Mar. 2016, doi: 10.1016/j.jmatprotec.2015.07.008.
- [3] D. J. Richardson, M. A. Keavey, and F. Dailami, "Modelling of cutting induced workpiece temperatures for dry milling," *Int J Mach Tools Manuf*, vol. 46, no. 10, pp. 1139–1145, Aug. 2006, doi: 10.1016/j.ijmachtools.2005.08.008.
- [4] M. J. Bermingham, S. Palanisamy, D. Morr, R. Andrews, and M. S. Dargusch, "Advantages of milling and drilling Ti-6Al-4V components with high-pressure coolant," *International Journal of Advanced Manufacturing Technology*, vol. 72, no. 1–4, pp. 77–88, 2014, doi: 10.1007/s00170-014-5666-1.
- [5] F. Fallenstein and J. C. Aurich, "CFD based investigation on internal cooling of twist drills," in *Procedia CIRP*, Elsevier, 2014, pp. 293–298. doi: 10.1016/j.procir.2014.03.112.
- [6] E. Uhlmann, H. Riemer, D. Schröter, F. Sammler, and S. Richarz, "Substitution of Coolant by Using a Closed Internally Cooled Milling Tool," in *Procedia CIRP*, Elsevier B.V., 2017, pp. 553–557. doi: 10.1016/j.procir.2016.11.267.
- [7] A. Johns, E. Merson, R. Royer, H. Thompson, and J. Summers, "A Numerical Investigation of Through-Tool Coolant Wetting Behaviour in Twist-Drilling," *J Fluid Flow Heat Mass Transf*, 2018, doi: 10.11159/jffhmt.2018.005.
- [8] R. Polvorosa, L. N. L. de Lacalle, A. J. S. Egea, A. Fernandez, M. Esparta, and I. Zamakona, "Cutting edge control by monitoring the tapping torque of new and resharpened tapping tools in Inconel 718," *International Journal of Advanced Manufacturing Technology*, vol. 106, no. 9–10, pp. 3799–3808, Feb. 2020, doi: 10.1007/s00170-019-04914-5.

- [9] C. W. Dai, W. F. Ding, Y. J. Zhu, J. H. Xu, and H. W. Yu, "Grinding temperature and power consumption in high speed grinding of Inconel 718 nickel-based superalloy with a vitrified CBN wheel," *Precis Eng*, vol. 52, pp. 192–200, Apr. 2018, doi: 10.1016/j.precisioneng.2017.12.005.
- [10] L. N. Lo Âpez De Lacalle, J. Pe Ârez, J. I. Llorente, and J. A. Sa Ânchez, "Advanced cutting conditions for the milling of aeronautical alloys."
- [11] N. Yin, G. Li, G. Tan, C. Shen, and J. Xue, "Design of the Feed Liquid System for an Internal Cooling End-milling," in *Journal of Physics: Conference Series*, Institute of Physics Publishing, Aug. 2018. doi: 10.1088/1742-6596/1064/1/012061.
- [12] Y. Su, N. He, L. Li, and X. L. Li, "An experimental investigation of effects of cooling/lubrication conditions on tool wear in high-speed end milling of Ti-6Al-4V," *Wear*, vol. 261, no. 7–8, pp. 760–766, Oct. 2006, doi: 10.1016/j.wear.2006.01.013.
- [13] A. Aggarwal, H. Singh, P. Kumar, and M. Singh, "Optimization of multiple quality characteristics for CNC turning under cryogenic cutting environment using desirability function," *J Mater Process Technol*, vol. 205, no. 1–3, pp. 42–50, Aug. 2008, doi: 10.1016/j.jmatprotec.2007.11.105.
- [14] A. Shokrani, V. Dhokia, and S. T. Newman, "Environmentally conscious machining of difficult-to-machine materials with regard to cutting fluids," 2012, *Elsevier Ltd.* doi: 10.1016/j.ijmachtools.2012.02.002.
- [15] V. Burnichon, C. Courbon, F. Salvatore, M. A. Cruz Gracia, U. Masciantonio, and J. Rech, "About the Possibility to Assess Cutting Fluids Efficiency Using an Instrumented Tribological Approach," *Materials Science Forum*, vol. 1147, pp. 125–132, Jul. 2025, doi: 10.4028/p-vhZ1nO.
- [16] M. A. E. Baradie, "Materials Processing Technology CUTTING FLUIDS: PART I. CHARACTERISATION," 1996.
- [17] X. Cui, F. Jiao, B. Zhao, and J. Guo, "A review of high-speed intermittent cutting of hardened steel," *International Journal of Advanced Manufacturing Technology*, vol. 93, no. 9–12, pp. 3837–3846, Dec. 2017, doi: 10.1007/s00170-017-0815-y.
- [18] K. Weinert, I. Inasaki, J. W. Sutherland, and T. Wakabayashi, "Dry Machining and Minimum Quantity Lubrication."

- [19] F. Klocke, D. Lung, T. Cayli, B. Döbbeler, and H. Sangermann, "Evaluation of energy efficiency in cutting aerospace materials with high-pressure cooling lubricant supply," *International Journal of Precision Engineering and Manufacturing*, vol. 15, no. 6, pp. 1179–1185, 2014, doi: 10.1007/s12541-014-0454-2.
- [20] K. Xu, Y. Yang, W. Feng, M. Wan, and W. Zhang, "Internal cooling techniques in cutting process: A review," *Journal of Advanced Manufacturing Science and Technology*, vol. 4, no. 4, 2024, doi: 10.51393/j.jamst.2024013.
- [21] R. Polvorosa, A. Suárez, L. N. L. de Lacalle, I. Cerrillo, A. Wretland, and F. Veiga, "Tool wear on nickel alloys with different coolant pressures: Comparison of Alloy 718 and Waspaloy," *J Manuf Process*, vol. 26, pp. 44–56, Apr. 2017, doi: 10.1016/j.jmapro.2017.01.012.
- [22] A. Suárez, F. Veiga, L. N. L. de Lacalle, R. Polvorosa, and A. Wretland, "An investigation of cutting forces and tool wear in turning of Haynes 282," *J Manuf Process*, vol. 37, pp. 529–540, Jan. 2019, doi: 10.1016/j.jmapro.2018.12.025.
- [23] C. Courbon, D. Kramar, P. Krajnik, F. Pusavec, J. Rech, and J. Kopac, "Investigation of machining performance in high-pressure jet assisted turning of Inconel 718: An experimental study," *Int J Mach Tools Manuf*, vol. 49, no. 14, pp. 1114–1125, 2009, doi: 10.1016/j.ijmachtools.2009.07.010.
- [24] X. Sun, R. Bateman, K. Cheng, and S. C. Ghani, "Design and analysis of an internally cooled smart cutting tool for dry cutting," *Proc Inst Mech Eng B J Eng Manuf*, vol. 226, no. 4, pp. 585–591, Apr. 2012, doi: 10.1177/0954405411424670.
- [25] C. Ferri, T. Minton, S. Bin Che Ghani, and K. Cheng, "Efficiency in contamination-free machining using microfluidic structures," *CIRP J Manuf Sci Technol*, vol. 7, no. 2, pp. 97–105, 2014, doi: 10.1016/j.cirpj.2013.12.001.
- [26] R. Peng, X. Huang, X. Tang, R. Chen, and Y. Hu, "Performance of a pressurized internal-cooling slotted grinding wheel system," *International Journal of Advanced Manufacturing Technology*, vol. 94, no. 5–8, pp. 2239–2254, Feb. 2018, doi: 10.1007/s00170-017-1014-6.
- [27] E. Oezkaya, N. Beer, and D. Biermann, "Experimental studies and CFD simulation of the internal cooling conditions when drilling Inconel 718," Sep. 01, 2016, *Elsevier Ltd.* doi: 10.1016/j.ijmachtools.2016.06.003.
- [28] X. Qin *et al.*, "A comparative study between internal spray cooling and conventional external cooling in drilling of Inconel 718," *International Journal of*

- *Advanced Manufacturing Technology*, vol. 104, no. 9–12, pp. 4581–4592, Oct. 2019, doi: 10.1007/s00170-019-04330-9.
- [29] W. Sales, M. Becker, C. S. Barcellos, J. Landre, J. Bonney, and E. O. Ezugwu, "Tribological behaviour when face milling AISI 4140 steel with minimum quantity fluid application," *Industrial Lubrication and Tribology*, vol. 61, no. 2, pp. 84–90, Mar. 2009, doi: 10.1108/00368790910940400.
- [30] H. Sasahara, T. Kikuma, R. Koyasu, and Y. Yao, "Surface grinding of carbon fiber reinforced plastic (CFRP) with an internal coolant supplied through grinding wheel," *Precis Eng*, vol. 38, no. 4, pp. 775–782, 2014, doi: 10.1016/j.precisioneng.2014.04.005.
- [31] D. O'sullivan and M. Cotterell, "Workpiece temperature measurement in machining," *Proc Inst Mech Eng B J Eng Manuf*, vol. 216, no. 1, pp. 135–139, 2002, Accessed: Sep. 09, 2025. [Online]. Available: https://doi.org/10.1243/0954405021519645
- [32] G.-C. Yang, S.-I. Ao, and L. Gelman, "Transactions on Engineering Technologies," in *World Congress on Engineering*, G.-C. Yang, S.-I. Ao, and L. Gelman, Eds., Springer Singapore, 2014. doi: https://doi.org/10.1007/978-981-10-1088-0.
- [33] M. Bräunig, L. Topinka, J. Regel, and M. Putz, "Special Interest Group Meeting on Thermal Issues Laboratory for Machine Tools and Production Engineering (WZL) of RWTH Aachen, Multi-phase numerical simulation of coolant flow around the cutting tool." [Online]. Available: www.euspen.eu
- [34] C. Naumann *et al.*, "INVESTIGATION OF TOOL COOLING AND HEAT TRANSFER USING COMPUTATIONAL FLUID DYNAMICS SIMULATIONS," *Journal of Machine Engineering*, vol. 24, no. 4, pp. 5–26, 2024, doi: 10.36897/jme/196074.
- [35] S. Brier, L. Topinka, J. Regel, and M. Dix, "Coupled fluid-structure-interaction simulation approach for correction of the thermal tool elongation to improve the milling precision," *Forschung im Ingenieurwesen/Engineering Research*, vol. 88, no. 1, Dec. 2024, doi: 10.1007/s10010-024-00751-5.
- [36] S. Brier *et al.*, "Coupled CFD model of tool environment and workspace to determine the convective heat transfer in jet cooling of milling processes in machine tools," in *Procedia CIRP*, Elsevier B.V., 2025, pp. 280–285. doi: 10.1016/j.procir.2025.02.049.

- [37] M. S. Najiha, M. M. Rahman, M. Kamal, A. R. Yusoff, and K. Kadirgama, "Minimum Quantity Lubricant Flow Analysis in End Milling Processes: A Computational Fluid Dynamics Approach," *Journal of Mechanical Engineering and Sciences*, vol. 3, pp. 340–345, Dec. 2012, doi: 10.15282/jmes.3.2012.10.0032.
- [38] M. S. Najiha and M. M. Rahman, "A computational fluid dynamics analysis of single and three nozzles minimum quantity lubricant flow for milling," *International Journal of Automotive and Mechanical Engineering*, vol. 10, no. 1, pp. 1891–1900, 2014, doi: 10.15282/ijame.10.2014.6.0157.
- [39] A. Duchosal, S. Werda, R. Serra, R. Leroy, and H. Hamdi, "Numerical modeling and experimental measurement of MQL impingement over an insert in a milling tool with inner channels," *Int J Mach Tools Manuf*, vol. 94, pp. 37–47, Jul. 2015, doi: 10.1016/j.ijmachtools.2015.04.003.
- [40] D. Biermann and E. Oezkaya, "CFD simulation for internal coolant channel design of tapping tools to reduce tool wear," *CIRP Ann Manuf Technol*, vol. 66, no. 1, pp. 109–112, 2017, doi: 10.1016/j.cirp.2017.04.024.
- [41] C. Zachert, H. Liu, T. Lakner, D. Schraknepper, and T. Bergs, "CFD simulation to optimize the internal coolant channels of an additively manufactured milling tool," in *Procedia CIRP*, Elsevier B.V., 2021, pp. 234–239. doi: 10.1016/j.procir.2021.09.040.
- [42] R. Peng, J. Liu, M. Chen, J. Tong, and L. Zhao, "Development of a pressurized internal cooling milling cutter and its machining performance assessment," *Precis Eng*, vol. 72, pp. 315–329, Nov. 2021, doi: 10.1016/j.precisioneng.2021.05.010.
- [43] T. Obikawa and M. Yamaguchi, "Computational fluid dynamic analysis of coolant flow in turning," in *Procedia CIRP*, Elsevier B.V., 2013, pp. 271–275. doi: 10.1016/j.procir.2013.06.101.
- [44] M. N. Morgan and V. Baines-Jones, "On the coherent length of fluid nozzles in grinding," *Key Eng Mater*, vol. 404, pp. 61–67, 2009, doi: 10.4028/www.scientific.net/kem.404.61.
- [45] T. Kelliger, H. Liu, D. Schraknepper, and T. Bergs, "Investigations on the Impact of Additively Manufactured Coolant Channels and Outlet Nozzles on Free Jet and Jet Forces in High-Pressure Cutting Fluid Supply-NC-ND license (http://creativecommons.org/licenses/by-nc-nd/4.0/) Peer review statement: Peer-review under responsibility of the scientific committee of the 21st

- Machining Innovations Conference for Aerospace Industry 2021." [Online]. Available: https://ssrn.com/abstract=3936402
- [46] S. Kugaevskii, E. Pizhenkov, and A. Gamberg, "The effectiveness of additive SLM-technologies in the manufacture of cutting tools," in *Materials Today: Proceedings*, Elsevier Ltd, 2019, pp. 1977–1981. doi: 10.1016/j.matpr.2019.07.055.
- [47] F. Klocke, B. Döbbeler, and T. Lakner, "Influence of the coolant nozzle orientation and size on the tool temperature under high-pressure coolant supply using an analogy test bench," *Production Engineering*, vol. 12, no. 3–4, pp. 473–480, Jun. 2018, doi: 10.1007/s11740-018-0823-2.
- [48] L. N. López De Lacalle, C. Angulo, A. Lamikiz, and J. A. Sánchez, "Experimental and numerical investigation of the effect of spray cutting fluids in high speed milling," *J. Mater. Process. Technol.*, vol. 172, no. 1, pp. 11–15, Feb. 2006, doi: 10.1016/j.jmatprotec.2005.08.014.
- [49] S. Roy and A. Ghosh, "High speed turning of AISI 4140 steel using nanofluid through twin jet SQL system," in *ASME 2013 International Manufacturing Science and Engineering Conference Collocated with the 41st North American Manufacturing Research Conference, MSEC 2013*, 2013. doi: 10.1115/MSEC2013-1067.
- [50] M. Hadad and B. Sadeghi, "Minimum quantity lubrication-MQL turning of AISI 4140 steel alloy," *J Clean Prod*, vol. 54, pp. 332–343, Sep. 2013, doi: 10.1016/j.jclepro.2013.05.011.
- [51] S. Ebbrell, N. H. Woolley, Y. D. Tridimas, D. R. Allanson, and W. B. Rowe, "The effects of cutting fluid application methods on the grinding process," 2000.
- [52] Kennametal, "HARVI™ Ultra 8X Helical Shell Mill SNHJ10 For Corner Radius 0,8-3,2mm Metric," https://www.kennametal.com/de/de/products/p.harvi-ultra-8x-helisel-freze-ic10-andnbspkovan-baglantl-metrik.6523850.html?srsltid=AfmBOoq0HGHVTx3z54jwnUcBkw8ArBZ9rIyueh vIzLWdS2rljgQo8Xjc.
- [53] S. Fienberg Irrgram Oll, *Springer Texts in Statistics Advisors*, Third., vol. 1. 1993.

 Accessed: Sep. 09, 2025. [Online]. Available: http://rd.springer.com/bookseries/417

- [54] S. Lecheler, "Conservation Equations of Fluid Mechanics," in *Computational Fluid Dynamics*, Springer Fachmedien Wiesbaden, 2022, pp. 13–45. doi: 10.1007/978-3-658-38453-1_2.
- [55] R. Peng, J. Liu, M. Chen, J. Tong, and L. Zhao, "Development of a pressurized internal cooling milling cutter and its machining performance assessment," *Precis Eng*, vol. 72, pp. 315–329, Nov. 2021, doi: 10.1016/j.precisioneng.2021.05.010.
- [56] B. Denkena, M. Mori, M. A. Dittrich, N. Klages, and J. Matthies, "Energy efficient supply of cutting fluids in machining by utilizing flow rate control," *CIRP Annals*, vol. 72, no. 1, pp. 349–352, Jan. 2023, doi: 10.1016/j.cirp.2023.04.082.
- [57] Werktuigen International, "Deckel Maho DMC 850V," https://www.werktuigen.com/deckel+maho-dmc+850v/wt-194-72861.
- [58] Seco Tools, "R217.97-1225.RE-X12.2A," https://www.secotools.com/article/p_02449582?productDetailsTab=fullSpecification&language=en.
- [59] Kennametal, "Kenna Universal™ Drill 5xD Internal Coolant Straight Shank Metric," https://www.kennametal.com/us/en/products/fam.kenna-universal-drill-5xd-internal-coolant-straight-shank-metric.100161493.html.
- [60] Gühring, "Ratio end mills Alu RF 100 AL / Ø 11.500 mm / Company std. / Solid carbide," https://webshop.guehring.de/en/00009082410115000.